Rapid Decadal Acceleration of Sea Level Rise along the U.S. East and Gulf Coasts during 2010–22 and Its Impact on Hurricane-Induced Storm Surge

Jianjun Yin[a]

[a] *Department of Geosciences, The University of Arizona, Tucson, Arizona*

ABSTRACT: Sea level rise (SLR) shows important spatiotemporal variability. A better understanding of characteristics and mechanisms of the variability is critical for future SLR projection and coastal preparedness. Here we analyze various observational and modeling data of sea level and its components, atmospheric pressure and winds, and ocean circulation in the North Atlantic. Both the century-long tide gauge data and the more recent altimetry data reveal a rapid decadal acceleration of SLR during 2010–22 along the U.S. East Coast and the Gulf of Mexico coast. The acceleration is most notable on the Southeast and Gulf Coasts, as quantified by the decadal rise rate, extreme annual sea level departure from the long-term trend, as well as the sea level record-breaking frequency and magnitude. Our analysis suggests that this SLR acceleration is largely a lagged response to the observed slowdown of the Atlantic meridional overturning circulation in 2009–10. In the North Atlantic, the response is characterized by a large-scale pattern of contrast changes in dynamic sea level between the Eastern Subpolar Gyre and the U.S. Southeast and Gulf Coasts. The latest global climate model generally captures this observed pattern and projects that further increase in greenhouse gas forcing will modify it over the twenty-first century. The faster SLR on the Southeast and Gulf Coasts, at a rate of more than 10 mm yr^{-1} during 2010–22, coincided with active and even record-breaking North Atlantic hurricane seasons in recent years. As a consequence, the elevated storm surge exacerbated coastal flooding and damage particularly on the Gulf Coast.

KEYWORDS: Sea level; Hurricanes/typhoons; Storm surges; Ocean circulation; Meridional overturning circulation; Climate change

1. Introduction

Sea level rise (SLR) is a major consequence of climate change (Wuebbles et al. 2017; Reidmiller et al. 2018; IPCC 2021). Its rate and magnitude are often quantified over a long period of time (e.g., 100 years). In addition to the long-term upward trend, sea level also shows shorter-term variability such as on the decadal time scale (Douglas et al. 2001; Zervas 2001; Sweet et al. 2022). In a changing climate, sea level variability could have both internal and forced components. Different driving mechanisms may be at play during different decades and at different locations. Thus, a better understanding of spatiotemporal characteristics and mechanisms of sea level variability and change, especially during the recent period, is critical for future SLR projections and coastal preparedness in the face of extreme events. With the advance of sea level observations and modeling, progress has been made recently so that SLR at different locations worldwide can be better explained and attributed (Fasullo et al. 2020; Hamlington et al. 2020; Harvey et al. 2021; Wang et al. 2021).

The densely populated U.S. East Coast and the Gulf of Mexico coast are vulnerable to SLR and extreme events. In the past six years, for example, major hurricanes and their associated storm surge have caused significant to catastrophic coastal flooding and socioeconomic damages especially along the Gulf Coast (NOAA 2022). Studying factors behind the increased coastal vulnerability, particularly the role of SLR in extreme events, is therefore urgently needed.

SLR along the East Coast and its time-evolving behaviors have been closely monitored and extensively studied. For example, using the long-term tide gauge data, Sallenger et al. (2012) reported a SLR hotspot on the Northeast coast during 1950–2009. Wdowinski et al. (2016) analyzed the 1998–2013 tide gauge data at Virginia Key, Florida, and detected an SLR acceleration after 2006. They found that the SLR acceleration correlated with the weakening of the Gulf Stream system and was responsible for the increased coastal flooding in Miami Beach. With the tide gauge data on the East Coast, Valle-Levinson et al. (2017) demonstrated an SLR deceleration (acceleration) north (south) of Cape Hatteras during 2011–15. They identified two modes of sea level variability and change related to the cumulative indices of ENSO and the North Atlantic Oscillation. Domingues et al. (2018) concluded that the 2010–15 SLR acceleration on the Southeast coast was mostly caused by the warming of the Florida Current. Ezer (2019) showed that the changes in the strength and latitudinal position of the Gulf Stream could cause SLR acceleration/deceleration in the Mid-Atlantic and South Atlantic Bight regions. Finally, Little et al. (2021) found multidecadal epochs of enhanced decadal sea level variability at the long East Coast tide gauge records.

With more years' data becoming available thus far, some of these previous results need to be updated and the mechanisms

---

TABLE 1. Observational and reanalysis datasets used in the present study.

	Dataset	Temporal frequency	Time span	Spatial resolution	Reference	Website
Sea/water level	Tide gauge	Monthly Hourly	1920–2022 1970–2022	Point measurement	Sweet et al. (2021), Zervas (2009)	https://tidesandcurrents.noaa.gov/
	Satellite altimetry	Monthly	1993–2021	0.25°	Pujol et al. (2016), Taburet et al. (2019)	https://marine.copernicus.eu/access-data
Ocean temperature and salinity	Levitus	Annual	1955–2022	1°	Levitus et al. (2012)	https://www.ncei.noaa.gov/access/global-ocean-heat-content/
Atmospheric pressure and wind	ERA5	Monthly	1959–2022	0.25°	Hersbach et al. (2020)	https://cds.climate.copernicus.eu/
AMOC transport	RAPID-AMOC	Twice-daily	2004–20	At 26°N of the North Atlantic	McCarthy et al. (2015), Bryden et al. (2020), Johns et al. (2011)	https://rapid.ac.uk/ https://mocha.rsmas.miami.edu/mocha/index.html
Tropical cyclone track	IBTrACS	3-hourly	1850–2022	Trajectory	Knapp et al. (2018, 2010)	https://www.ncei.noaa.gov/products/international-best-track-archive

for the recent sea level behaviors need to be revisited. In addition, the latest generation of the atmosphere–ocean general circulation model offers new insights about the cause of sea level variability and change on the East and Gulf Coasts. Thus, in this study, we take advantage of various datasets as described in section 2 and focus on observed and modeled sea levels in the North Atlantic and along the entire East and Gulf Coasts of the U.S. With the tide gauge and altimetry data, we identify a rapid SLR acceleration on the East and Gulf Coasts during 2010–22 (section 3a). For the first time, we link the SLR acceleration on the Southeast and Gulf Coasts to the observed 2009–10 slowdown of the Atlantic meridional overturning circulation (AMOC) (section 3b). To put the recent behavior of sea level into context, we show the sea level simulation and projection by the latest climate model over the satellite era and the twenty-first century (section 3c). Last, we evaluate the impact of the 2010–22 SLR acceleration on hurricane-induced storm surge along the Southeast and Gulf Coasts (section 3d). Our systematic analysis on the sea/water level data here covers a broad spectrum of time scales, ranging from hourly, daily, monthly, yearly, to decadal and centennial.

2. Data, model, and methods

Table 1 summarizes the observational and reanalysis datasets used in this study. More specific information about these datasets and a brief model description are given below.

a. Tide gauge data

The long-term monthly tide gauge data for the relative sea level along the U.S. East and Gulf Coasts are obtained from the NOAA Tides and Currents (Zervas 2009; Sweet et al. 2021). The location of the tide gauge stations and their data length are shown in Fig. 1 and listed in Table S1 in the online

supplemental material. With the monthly data, we first calculate the annual mean sea level at each station. Given the gaps in the data, any year with missing data for more than three months is not used.
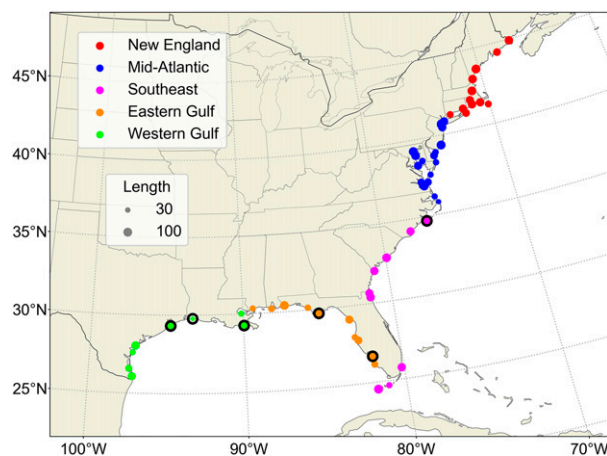

FIG. 1. Tide gauge stations along the U.S. East and Gulf Coasts. Different colors indicate different regions: New England (north of New York), mid-Atlantic (between New York and Cape Hatteras), Southeast (between Cape Hatteras and Key West), and eastern and western Gulf (east and west of New Orleans, respectively). Different dot sizes indicate different data lengths in years. Of the 58 stations, 12 are in New England, 19 in the mid-Atlantic, 9 in the Southeast, 10 on the eastern Gulf, and 8 on the western Gulf. See Table S1 for more information about these tide gauge stations, their sea level data, and SLR rates. The black circles mark the six stations along the Southeast and Gulf Coasts used for the storm surge study (Figs. 12–15). Of the six stations, one is on the Southeast coast (Beaufort) and the other five are on the Gulf Coast (Fort Myers, Apalachicola, Grand Isle, Calcasieu Pass, and Galveston Pier 21).
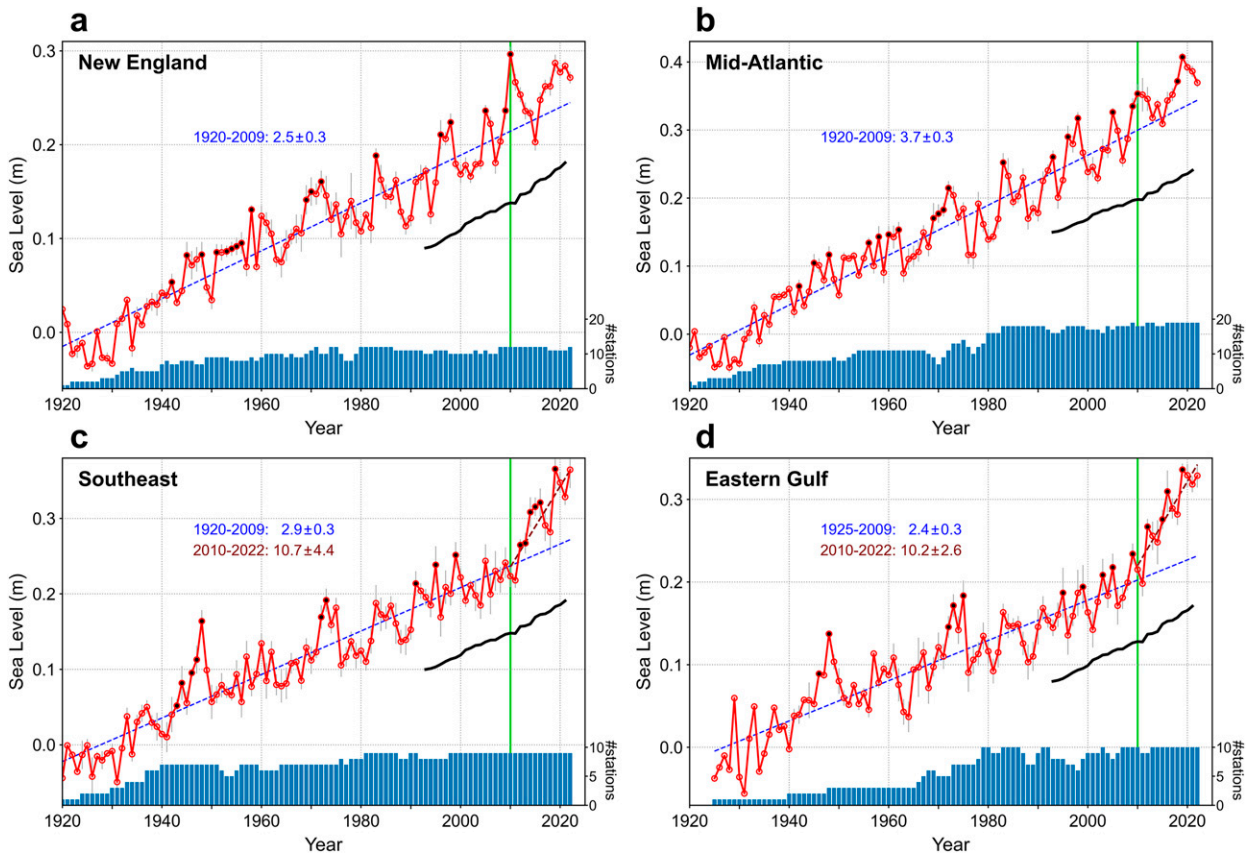
FIG. 2. SLR along the U.S. East and Gulf Coasts from the century-long tide gauge data (1920–2022). (a) New England, (b) mid-Atlantic, (c) Southeast, and (d) eastern Gulf. The red curves are the mean of the tide gauge data in the same region relative to the period of 1920–40. The number of tide gauge stations used for calculating the regional mean is shown by the blue bars at the bottom of each panel. The blue dashed line is the linear regression for sea level during 1920–2009. It is extrapolated to 2022 to show the sea level departure during 2010–22. For (c) and (d), the linear regression for the 2010–22 period is also plotted (brown dashed lines). The mean rise rate (mm yr^{-1}) and its 95% confidence interval are listed. The vertical error bars in gray show the standard deviation ($\pm 1\sigma$) of Δh_i across stations in the same region [Eq. (1)]. The black dots mark sea level records after 1940. The black solid line is the global mean SLR during 1993–2021 from the altimetry data. The vertical green line marks the year 2010.

The correlations among different stations reveal three regimes of sea level variability and change: the Northeast, Southeast, and Gulf Coasts (Fig. S1). In each region, the coastal sea levels are coherent and correlated with the sea level on the shelf. According to these sea level correlations as well as different SLR rates (Table S1), we divide the East and Gulf Coasts into five regions: New England, the mid-Atlantic, Southeast, and eastern and western Gulf (Fig. 1). Due to land subsidence in the western Gulf (Wang et al. 2020), we use the stations in the eastern Gulf to study the absolute SLR along the Gulf Coast.

To compute the regional mean sea level, we differentiate the annual sea level for each station (Δh_i) and then average Δh_i for all available stations in the same region:

$$\Delta h_i(t) = h_i(t) - h_i(t-1), \qquad (1)$$

$$\overline{\Delta h}(t) = \frac{1}{n} \sum_{i=1}^{n} \Delta h_i(t), \qquad (2)$$

$$i = 1, \ldots, n; \ t = 1920, \ldots, 2022,$$

where i and n denote the station index and the number of stations in the same region, respectively. As the stations are distributed generally evenly in the same region, we adopt an unweighted average of Δh_i [Eq. (2)]. Then we calculate the running sum of $\overline{\Delta h}$ to obtain the regional mean sea level curve. The standard deviation of Δh_i across stations is used to evaluate the uncertainty associated with the regional mean. The SLR rate is computed based on the linear trend of the sea level curves. Its 95% confidence interval is quantified by using an autoregressive model of the residuals (Zervas 2009).

In addition to the monthly sea level data, we also use the hourly water level data from the NOAA Tides and Currents to study the impact of the 2010–22 SLR acceleration on recent hurricane-induced storm surge along the Southeast and Gulf Coasts. We use the data at six tide gauge stations: Galveston Pier 21 in Texas to study the surge induced by Hurricane Harvey in 2017, Beaufort in North Carolina for Hurricane Florence in 2018, Apalachicola in Florida for Hurricane Michael in 2018, Calcasieu Pass in Louisiana for Hurricane Laura in
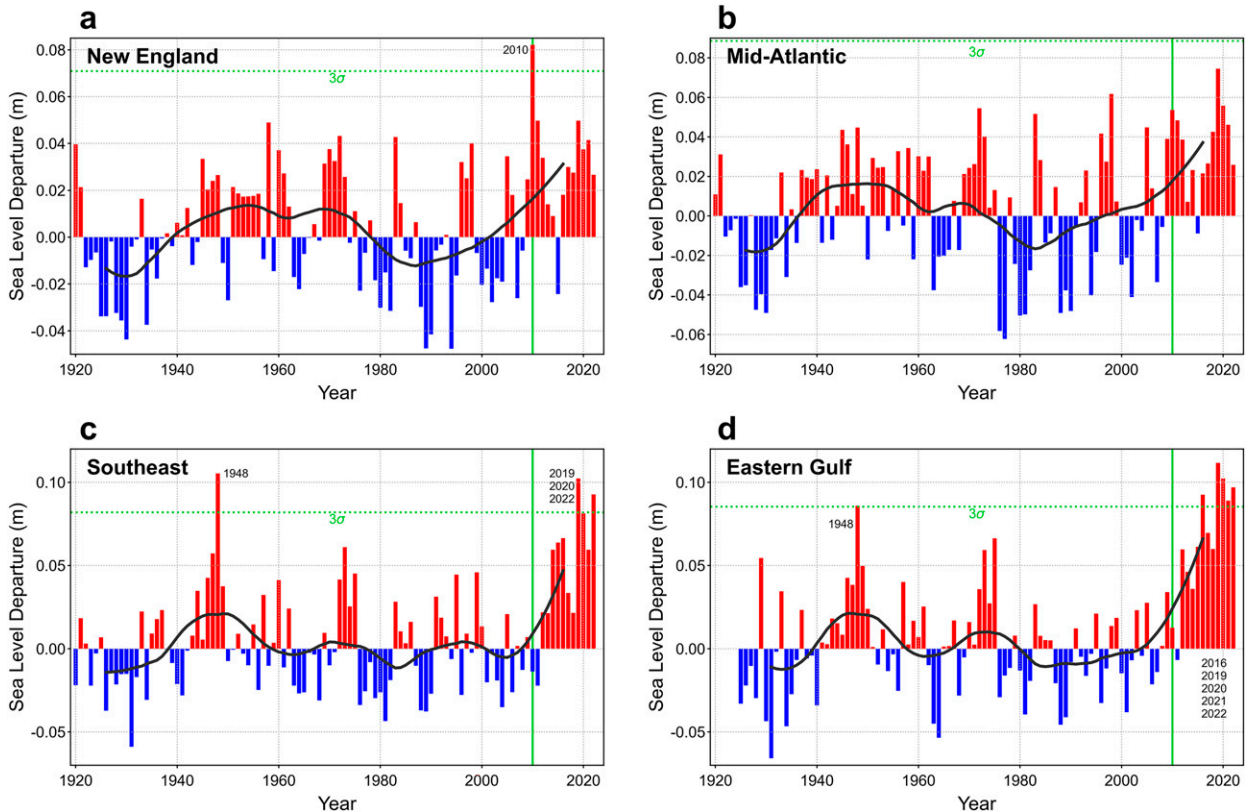
FIG. 3. Departure of annual sea levels from their long-term linear trends along the U.S. East and Gulf Coasts. (a) New England, (b) mid-Atlantic, (c) Southeast, and (d) eastern Gulf. The linear trend is calculated based on the 1920–2009 period (Fig. 2). The horizontal dotted lines in green mark 3σ of the annual sea level departure. The years with a $\geq 3\sigma$ sea level departure are labeled. The black curves are the 13-yr running mean of the sea level departure. The vertical green line marks 2010.

2020, Grand Isle in Louisiana for Hurricane Ida in 2021, and Fort Myers in Florida for Hurricane Ian in 2022 (Fig. 1). All the six hurricanes in the past six years were high-impact category 4–5 storms. Each of them caused $27–$152 billion in damages (NOAA 2022).

b. Satellite altimetry data

The altimetry data are obtained from the Copernicus Marine Environment Monitoring Service (Pujol et al. 2016; Taburet et al. 2019). The delayed-time products at a monthly frequency span from January 1993 to December 2021 and have a spatial resolution of 0.25°. The near-real-time daily data are used to estimate sea levels in 2022. In the altimetry data, sea level anomalies are computed with respect to the 1993–2012 mean. The data quality in the coastal regions has been improved recently (Taburet et al. 2019). Unlike the tide gauge data, the altimetry data are geocentric measurements of sea level and therefore not influenced by land vertical movement. In addition, the inverse barometer effect has been removed in the altimetry data while the glacial isostatic adjustment correction is not applied. The global mean SLR in the altimetry data is calculated as

$$\overline{\text{SLA}}(t) = \frac{1}{A}\int_A \text{SLA}(x, y, t)dA, \quad t = 1993, \ldots, 2021, \quad (3)$$

where SLA and $\overline{\text{SLA}}$ are the annual sea level anomaly and its global mean, respectively; A is global ocean surface areas excluding the sea ice coverage regions. Dynamic sea level (DSL; see appendix A) in the altimetry data is computed as

$$\text{SLA}'(x, y, t) = \text{SLA}(x, y, t) - \overline{\text{SLA}}(t), \quad t = 1993, \ldots, 2021. \quad (4)$$

The prime term denotes the departure from the global mean. So, by definition, DSL always has a zero global mean.

c. Levitus data for steric, thermosteric, and halosteric sea levels

The dataset with a 1° resolution from the NOAA NCEI is referred to as the Levitus data (Levitus et al. 2012). The annual steric, thermosteric and halosteric sea level anomalies for the upper 2000 m ocean are available for 2005–22. They are computed based on observed three-dimensional ocean temperature and salinity anomalies such as from Argo (see appendix A). The ocean temperature and thermosteric sea level anomalies for the upper 700 m ocean are available for a longer period (1955–2022). For the interior ocean in the North Atlantic, the steric, thermosteric and halosteric sea
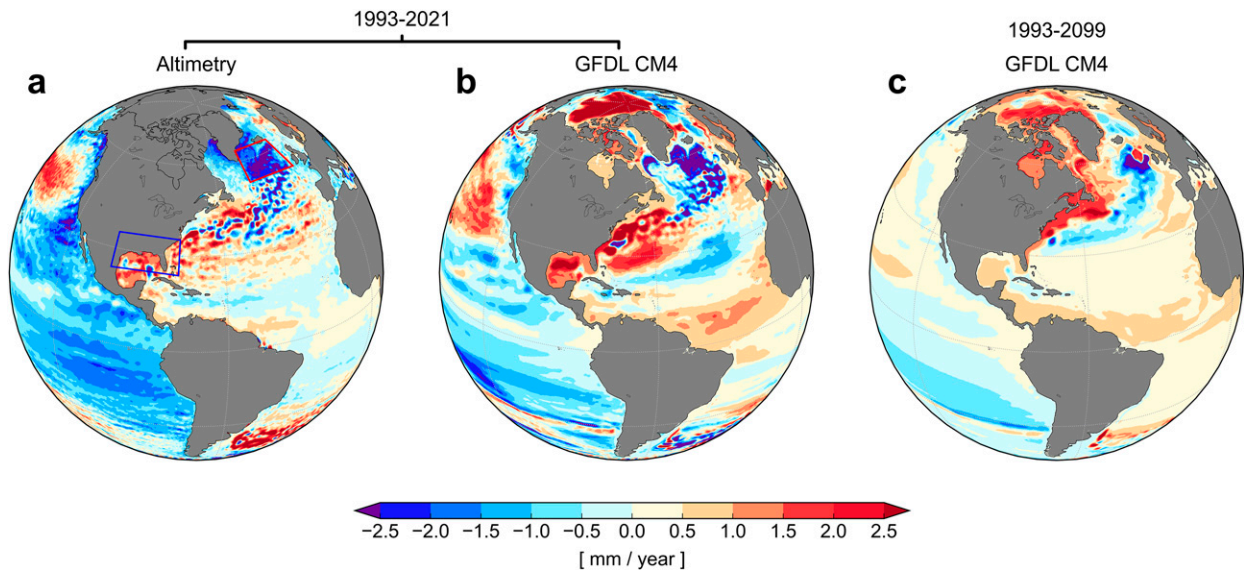
FIG. 4. Linear trend of DSL in the North Atlantic and along the U.S. East and Gulf Coasts. (a) Satellite altimetry data during 1993–2021. (b) Multidecadal trend (1993–2021) in the simulation and projection of the GFDL CM4 climate model. (c) Centennial trend (1993–2099) in the model. In (b) and (c), the historical simulation (1993–2014) is combined with the SSP245 projection (2015–21 or 2015–99) to derive these trends. In (a), the sea ice coverage region in the Arctic Ocean is masked out. The red and blue boxes highlight the contrast changes between the Eastern Subpolar Gyre (13°–42°W, 52°–64°N) and the U.S. Southeast and Gulf Coasts. Note that the global mean SLR is removed in all panels.

level anomalies of the entire ocean column are dominated by the upper 700-m ocean layer (see section 3b).

d. ERA5 reanalysis data for atmospheric forcing

To study the role of atmospheric forcing in the SLR acceleration during 2010–22, we use the monthly data of ERA5 for sea level pressure and the zonal and meridional winds at 10 m and wind stress. ERA5 reanalysis has a 0.25° resolution globally and covers the period of 1959–2022 (Hersbach et al. 2020).

e. Observed AMOC transports at 26°N of the North Atlantic

Starting from 2004, the RAPID-AMOC Programme has been measuring the AMOC volume and heat transports at 26°N of the North Atlantic at a twice-daily frequency (McCarthy et al. 2015). The time series of the AMOC volume transport have recently been updated to December 2020. The northward heat transport across 26°N of the North Atlantic is available for the 2004–18 period (Johns et al. 2011; Bryden et al. 2020).

f. Tropical cyclone tracks in the North Atlantic

The observed tracks of tropical cyclones are based on the International Best Track Archive for Climate Stewardship (IBTrACS) (Knapp et al. 2010, 2018). IBTrACS provides storm intensity and position at 3-hourly intervals. Storm intensity is categorized with the Saffir–Simpson hurricane scale (Simpson and Saffir 1974). Categories 1–5 are based on the hurricane's maximum sustained wind speed, but without considering other impacts such as storm surge, rainfall, and tornadoes.

g. The GFDL CM4 global climate model

CM4 is the latest generation of the coupled atmosphere–ocean general circulation model developed and used at the Geophysical Fluid Dynamics Laboratory (GFDL) of NOAA (Held et al. 2019). The atmospheric model adopts finite-volume cubed-sphere dynamical core with 96 grid boxes per cube face (~1° grid spacing). It has 33 vertical levels with the model top at 1 hPa. The oceanic model of CM4 is based on the Modular Ocean Model, version 6 (MOM6), and has a 0.25° eddy-permitting horizontal resolution. It combines geopotential and isopycnal vertical coordinates and has 75 hybrid vertical layers.

CM4 has been used at GFDL to carry out the standard CMIP6 experiments, including the historical simulation for the 1850–2014 period and the twenty-first-century projections (2015–99) under the medium and high Shared Socioeconomic Pathways (SSP245 and SSP585) emission scenarios (Eyring et al. 2016; O'Neill et al. 2016). DSL is a direct model output variable in CM4. A previous model evaluation (Yin et al. 2020) indicates that compared with the altimetry data, CM4 simulates the mean, seasonal cycle, and interannual variability of DSL reasonably well. The model simulation data can be found at the CMIP6 archive (https://esgf-node.llnl.gov/projects/cmip6/).

3. Results

a. Observed SLR acceleration during 2010–22

The tide gauge data since 1920 show that SLR along the U.S. East and Gulf Coasts was roughly linear prior to 2010, superimposed by interannual and decadal variability (Fig. 2).
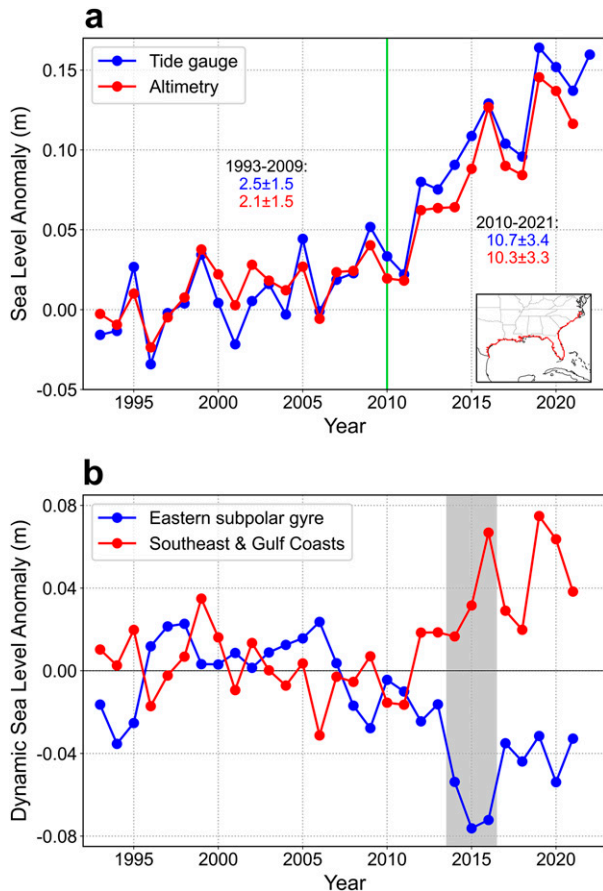
Fig. 5. Sea level changes in the tide gauge and altimetry data during 1993–2021. (a) Comparison of the regional mean SLR along the Southeast and Gulf Coasts between the tide gauge and altimetry data. The global mean SLR is included. The numbers in color compare the linear rise rates (mm yr^{-1}) between the two datasets for the 1993–2009 and 2010–21 periods. For the tide gauge data, the stations in the Southeast and eastern Gulf are used (Fig. 1). For the altimetry data, the coastal ocean grid points (red color in the inset) are averaged for the regional mean. The two curves are calibrated for a better comparison and the difference between them is partly due to land subsidence included in the tide gauge data (Karegar et al. 2016; Wang et al. 2020). (b) Contrast and concurrent changes in DSL (the global mean SLR removed) between the Eastern Subpolar Gyre (see the red box in Fig. 4a) and along the U.S. Southeast and Gulf Coasts [see the inset in (a)]. The gray shading highlights the divergence of the two curves in 2014–16.

The linear rise rates during 1920–2009 are 2.5 ± 0.3, 3.7 ± 0.3, 2.9 ± 0.3, and 2.4 ± 0.3 mm yr^{-1} (mean and 95% confidence interval) in the New England, mid-Atlantic, Southeast, and eastern Gulf regions, respectively.

Since 2010, SLR has been undergoing a rapid acceleration on the U.S. Southeast and Gulf Coasts. The 2010–22 linear rise rates increased to 10.7 ± 4.4 and 10.2 ± 2.6 mm yr^{-1} on the Southeast and eastern Gulf Coasts, respectively (Figs. 2c,d). It should be noted that the decadal- and centennial-time-scale SLR rates are not directly comparable. We use the decadal rate here to quan-
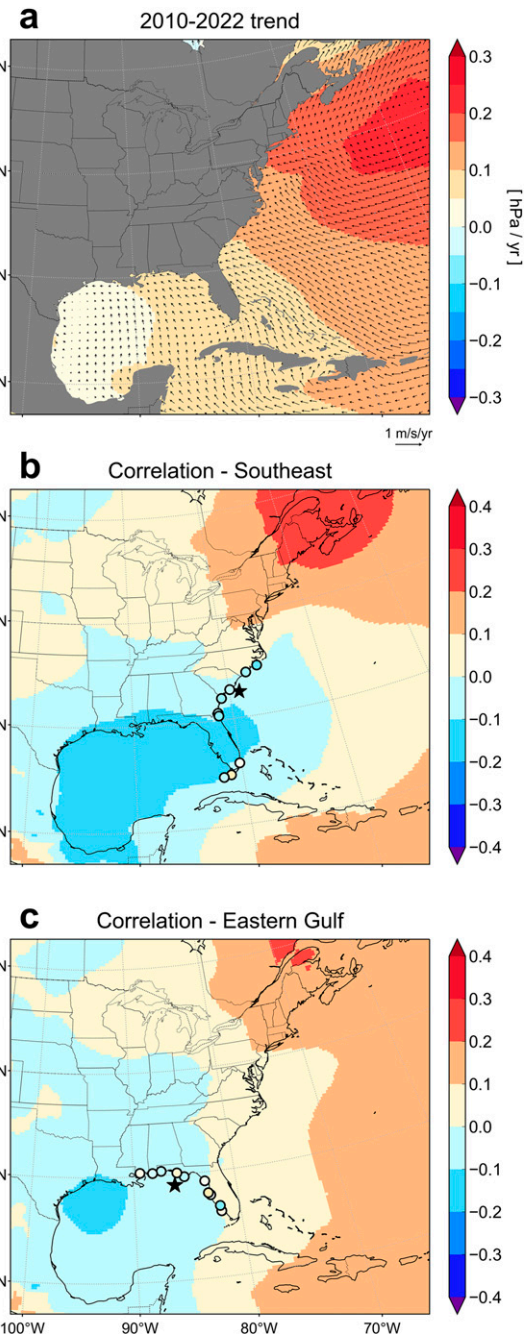
Fig. 6. Role of local atmospheric forcing in the 2010–22 SLR acceleration along the Southeast and eastern Gulf Coasts. (a) 2010–22 linear trends of sea level pressure (shading) and winds (vectors) in the western North Atlantic (ERA5). (b) Correlation (1959–2022) between the annual sea level departure from the long-term trend along the Southeast coast and the atmospheric pressure anomalies. (c) As in (b), but for the eastern Gulf Coast. The shading is the correlation of the regional mean sea level departure time series (i.e., Figs. 3c,d) with the detrended atmospheric pressure anomalies from ERA5. The colored circles are the local correlation at each tide gauge station. The black star marks the location of the nearby wind used for Fig. 7. See Fig. S4 for the correlation during 1959–2009.
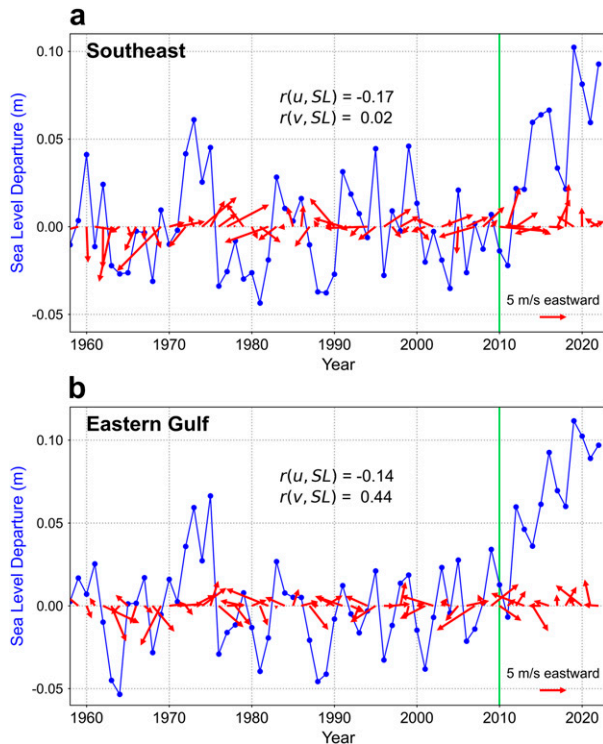
FIG. 7. Stick plot of the wind anomalies (speed and direction; red arrows) near the Southeast and eastern Gulf Coasts and the coastal sea level variability. The wind is taken from a site just offshore of Charleston or Pensacola (see the black stars in Figs. 6b,c). The annual wind anomalies are relative to the 1959–2022 mean. The blue lines are the coastal sea level departure from the long-term linear trend (Figs. 3c,d). The correlation coefficients (r) between the annual sea level departure (SL) and the anomalies of the nearby eastward and northward wind (u and v, respectively) are computed and listed.

tify the speed of the sea level divergence during 2010–22 from the long-term linear trend. On the Southeast coast, the SLR acceleration is generally consistent with what has been reported previously (Wdowinski et al. 2016; Valle-Levinson et al. 2017; Domingues et al. 2018; Ezer 2019). Importantly, we show here that the acceleration has extended to the Gulf Coast.

During the past decade, sea levels in three years (2019, 2020, and 2022) show a $\geq 3\sigma$ departure from the long-term trend on the Southeast coast, and five years (2016, 2019, 2020, 2021, and 2022) on the eastern Gulf (Figs. 3c,d). Here, σ denotes the standard deviation of the annual sea levels with the long-term linear trend removed. A value of 3σ is set as the criterion to identify extreme annual sea levels. The $\geq 3\sigma$ departure occurred only once (1948) prior to 2010. The decadal (13 yr) running mean can reveal longer-time-scale variability (black curves in Fig. 3). Compared with the twentieth-century sea level variations around the linear regression line, the 2010–22 SLR acceleration is unprecedented, especially on the Gulf Coast (Fig. 3d).

The accelerated SLR is also evidenced by the sea level records being broken more frequently in the past decade, and by the record-breaking magnitude (Figs. 2c,d). During 2010–22, six and four new records have been set on the Southeast and eastern Gulf Coasts, respectively. On average, the records had
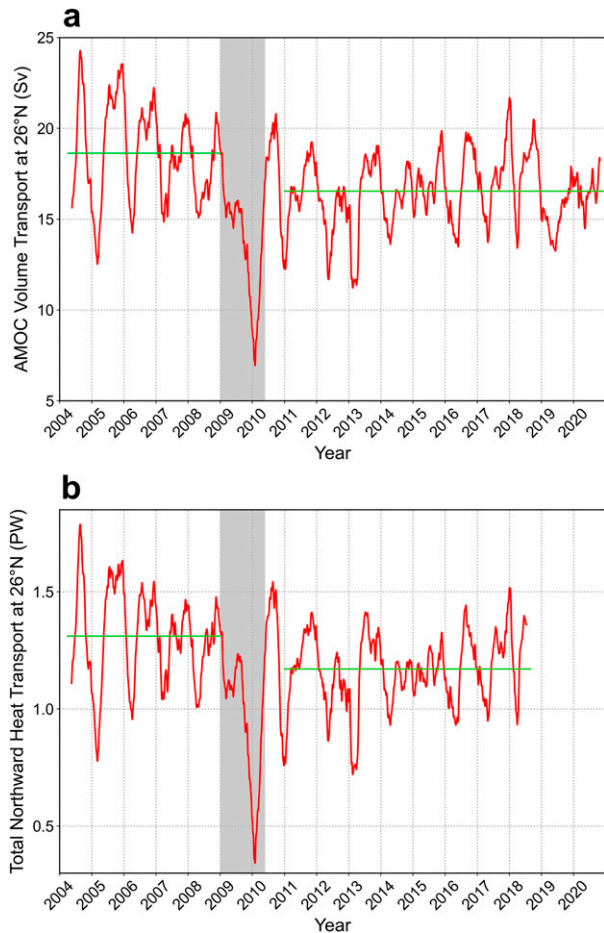
FIG. 8. Time series of the observed AMOC volume transport and the total northward heat transport at 26°N in the North Atlantic. (a) 3-month running mean of the AMOC volume transport from the RAPID AMOC program. (b) 3-month running mean of the total northward heat transport. The 2009–10 AMOC slowdown event is highlighted by the gray shading. The horizontal green lines indicate the mean values before and after the 2009–10 event (i.e., during 2004–08 and 2011–20/2011–18).

been broken by 1.5 times per decade during 1940–2009. The latest record set in 2019 was 0.11 and 0.10 m higher than the pre-2010 record on the Southeast (1999) and eastern Gulf (2009), respectively. Thus, the 2010–22 linear trend (≥ 10 mm yr^{-1}) and the record-breaking magnitudes (≥ 0.10 m) are consistent in quantifying the SLR acceleration (Figs. 2c,d).

The satellite altimetry data since 1993 confirm the 2010–22 SLR acceleration in both its timing and rate along the Southeast and Gulf Coasts (Figs. 4a and 5a). The altimetry data also confirm that the western Gulf Coast experienced an acceleration of the absolute SLR similar to that on the eastern Gulf Coast. The acceleration on the Southeast and Gulf Coasts was preceded by a period of slow rise rates during 1990–2009, suggesting that a quick switch of SLR modes had occurred around 2009–10 (Figs. 2c,d and 5a).

Sea level along the U.S. Northeast coast, including both the New England and mid-Atlantic regions, was also higher
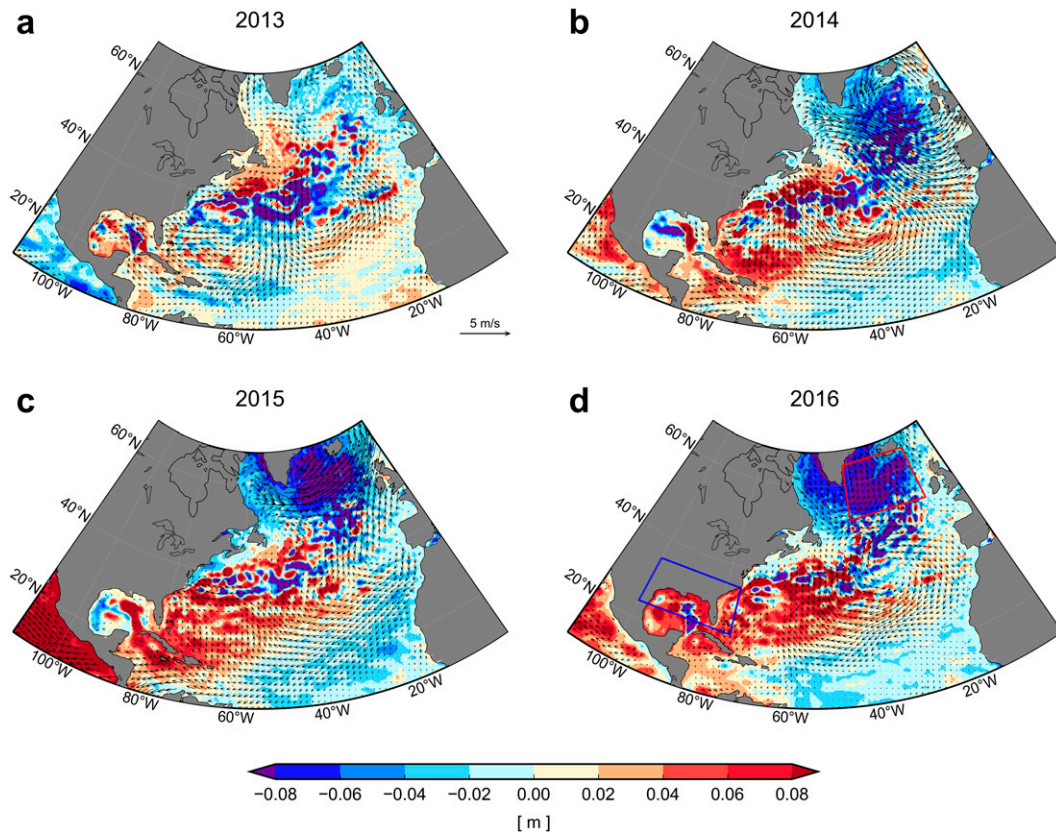
FIG. 9. Adjustment of DSL in the North Atlantic in response to the 2009–10 AMOC slowdown. Color shading and vectors indicate DSL (altimetry) and wind (ERA5) anomalies, respectively, for (a) 2013, (b) 2014, (c) 2015, and (d) 2016. In (d) the red and blue boxes highlight the contrast changes in DSL between the Eastern Subpolar Gyre and the U.S. Southeast and Gulf Coasts.

during 2010–22 and overall above the long-term trend line except in 2015 (Figs. 2a,b). The mean sea level departure during 2010–22 from the long-term trend is 3.0 and 3.7 cm on the New England and mid-Atlantic coasts, respectively (Figs. 3a,b). The higher coastal sea level was accompanied by a rapid transition of the nearby shelf oceans into a warmer state since 2010 (Pershing et al. 2015; Neto et al. 2021). The volume mean ocean temperatures on the shelf near the New England coast warmed by 1.4°C during 2010–22 compared with 2000–09 (Fig. S2). This implies that more waters of subtropical origin have since been present on the shelf. The sea level spike in 2010 on the New England coast represents the largest and the only ≥3σ annual departure from the long-term trend line (Fig. 3a) (Goddard et al. 2015). Despite the continuous global SLR during the past decade, the 2010 sea level record has not been broken yet as of 2022 (Fig. 2a).

b. Mechanisms of the 2010–22 SLR acceleration

The global mean SLR from altimetry, with a linear trend of 3.2 ± 0.2 and 4.0 ± 0.3 mm yr^{-1} during 1993–2021 and 2010–21, respectively, falls short to explain the rapid decadal acceleration on the Southeast and Gulf Coasts (Figs. 2c,d).

In terms of the atmospheric forcing, sea level pressure from the ERA5 reanalysis shows a slight increase trend at the midlatitude North Atlantic during 2010–22 (Fig. 6a and Fig. S3). This change generated anomalous onshore winds near the Southeast and Gulf Coasts. However, a further and detailed analysis indicates a weak correlation between the 2010–22 SLR acceleration and the anomalies of the nearby wind and local atmospheric pressure. Prior to the rapid SLR acceleration and over 1959–2009, the detrended coastal sea level and atmospheric pressure show a weak negative correlation on the Southeast and eastern Gulf Coasts ($|r| \leq |-0.4|$) (Fig. S4). Including the 2010–22 period further reduces the correlation to $|r| < |-0.2|$ over 1959–2022 (Figs. 6b,c).

These weak correlations suggest that the inverse barometer effect associated with the atmospheric pressure anomalies is not a primary driver of the coastal sea level variability and change, contradicting the finding by Piecuch and Ponte (2015). The correlation between the annual sea level departure on the Southeast coast and the nearby eastward wind anomalies is -0.17 during 1959–2022 (Fig. 7a). On the eastern Gulf Coast, the correlation of the sea level departure with the northward wind anomalies is somewhat higher ($r = 0.44$ with p value = 0.00) (Fig. 7b).

In addition to the local atmospheric forcing, the wind can influence coastal sea levels remotely through the southward Sverdrup transport and the compensating northward Gulf

Stream transport. According to the wind stress curl from the ERA5 reanalysis data, the southward Sverdrup transport across 30°N in the North Atlantic shows no significant deviation during 2010–22 from its previous variability (Figs. S3 and S5). Thus, the atmospheric pressure and wind are unlikely to have caused the 2010–22 SLR acceleration on the Southeast and Gulf Coasts.

Instead, the acceleration appears to be a regional manifestation of the large-scale DSL adjustment in the North Atlantic in response to the observed slowdown of the AMOC in 2009–10 (Fig. 8a) (Bryden et al. 2014; Smeed et al. 2014). The pattern of the DSL adjustment is characterized by opposite changes between the Eastern Subpolar Gyre and the Western Subtropical Gyre including the Gulf of Mexico and the Caribbean Sea (Figs. 4a and 9d). The 2009–10 AMOC slowdown caused a reduction of the northward heat/salt transport in the North Atlantic (Fig. 8b) (Bryden et al. 2020). The resultant cooling/freshening of the subpolar North Atlantic led to a depression of DSL through the thermosteric effect, partially compensated by the halosteric effect (Fig. S6) (Rahmstorf et al. 2015; Chafik et al. 2019; Chemke et al. 2020).

The process of the DSL adjustment is evident during 2013–16. In 2013, DSL was higher (lower) north (south) of the Gulf Stream downstream of Cape Hatteras (Fig. 9a). In 2014, a negative DSL region started to emerge around 50°N of the North Atlantic (Fig. 9b). DSL deepened further during 2015–16 and the negative region migrated further northward to the Eastern Subpolar Gyre around 60°N (Figs. 9c,d). The maximum DSL fall in the Eastern Subpolar Gyre was up to 0.1 m, lagging the 2009–10 AMOC slowdown at 26°N by a few years.

Meanwhile, ocean heat accumulation and dynamical adjustments at the lower latitudes raised DSL in the Gulf of Mexico and the Sargasso Sea, south of the Grand Banks, as well as along the U.S. Southeast and Gulf Coasts (Figs. 4a, 5b and 9) (Ezer 2015; Domingues et al. 2018; Fasullo and Nerem 2018; Neto et al. 2021). According to Figs. 5b and 9, the DSL rise on the southeast coast started in 2014 and was concurrent with the DSL fall in the Eastern Subpolar Gyre. The DSL rise extended to the Gulf Coast in 2016. In 2015 and 2016, the atmospheric pressure and wind anomalies near the Southeast and Gulf Coasts were weak (Figs. 9c,d). Again, this suggests that the high coastal sea levels in the two years were not caused by the local atmospheric pressure and wind effect. Instead, the concurrent, divergent, and contrast changes in DSL between the subpolar and subtropical regions is strong evidence of the 2010–22 SLR acceleration along the Southeast and Gulf Coasts intrinsically linked to the 2009–10 AMOC slowdown.

To put this large-scale, decadal pattern of DSL changes into a long-term context, we use NOAA's ocean temperature and the thermosteric sea level data that go back to 1955 (Levitus et al. 2012). In the North Atlantic, the variation and change of the steric and thermosteric sea levels are highly correlated ($r > 0.9$) and dominated by anomalies in the upper 700 m (Fig. S6). EOF1 of the thermosteric sea level without the global mean shows a pattern of contrast changes between the subpolar and subtropical gyres in the North Atlantic during 1955–2022 (Fig. 10). In addition to the interannual to multidecadal variability, there is a secular upward trend of PC1
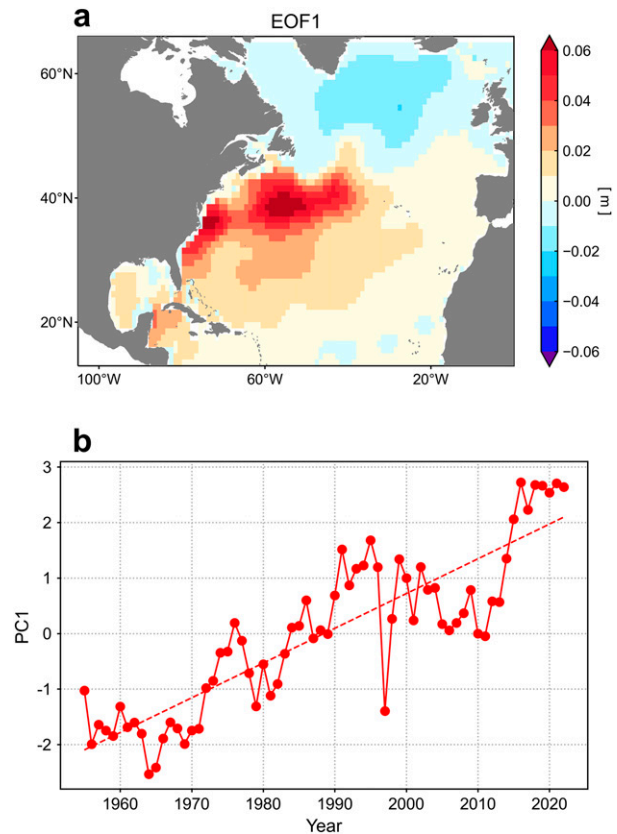

FIG. 10. EOF1 and PC1 of the thermosteric sea level (Levitus data for the upper 700-m ocean) in the North Atlantic during 1955–2022. The EOF analysis is performed over the North Atlantic (100°W–0°, 15°–65°N) with the global mean thermosteric SLR removed. The dashed line in (b) is the linear trend of PC1. See Fig. S7 for EOF2/PC2.

suggesting a sea level fall and rise due to the temperature effect in the subpolar and subtropical gyres, respectively. The rapid and unprecedented increase in PC1 during 2014–16 is particularly pronounced, and consistent with the altimetry data (Figs. 4a and 9). Unlike EOF1, EOF2 shows a pattern of opposing changes between the Slope Sea region and the eastern and northern North Atlantic (Fig. S7). EOF1 and EOF2 explain 37% and 12% of the total variance, respectively.

c. Model simulations and projections

Thanks to the new development and improvement, the latest atmosphere–ocean general circulation model captures the observed pattern of DSL changes in the North Atlantic over the satellite era. Compared with previous model generations, the refined model resolution and improved model physics and dynamics in the GFDL CM4 lead to better simulations of the jetlike Gulf Stream and associated sharp DSL gradient just offshore of the Southeast coast (Yin et al. 2020). By combining the historical simulation (1993–2014) and the projection under the medium SSP245 emission scenario (2015–21), CM4 simulates a DSL fall in the Eastern Subpolar Gyre during 1993–2021
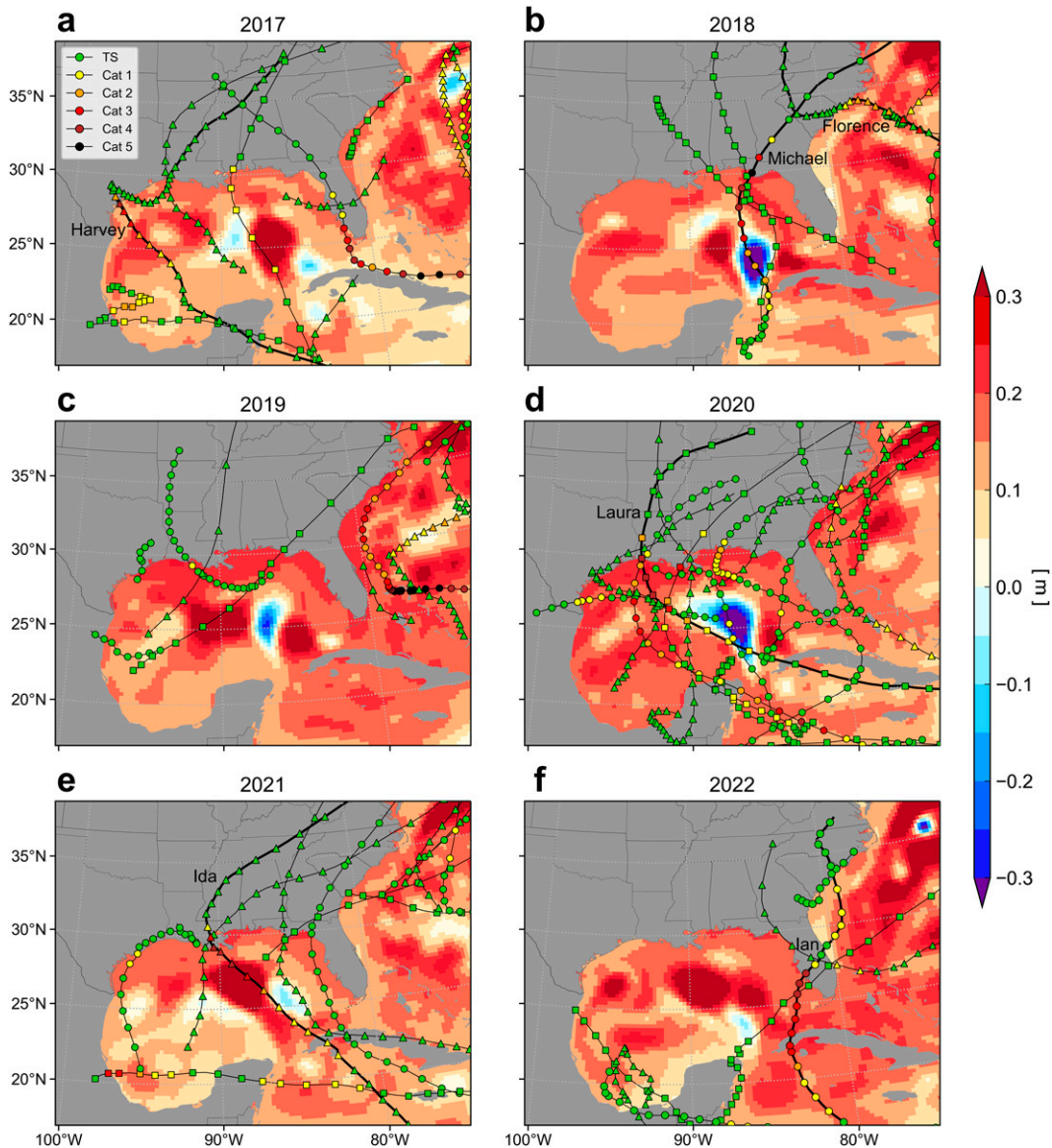
FIG. 11. Higher sea levels and active hurricane seasons in recent years. (a)–(f) Hurricane activities in 2017–22. The lines with color-filled symbols (circles, rectangles, and triangles) are observed tropical cyclone storm tracks from IBTrACS, plotted at 6-hourly intervals. The color of the symbols denotes storm intensity, ranging from tropical storm (TS) to category 1–5 hurricanes. Six high-impact hurricanes are highlighted by thick black lines: Hurricanes Harvey in 2017, Florence in 2018, Michael in 2018, Laura in 2020, Ida in 2021, and Ian in 2022. The color shading shows the hurricane season (July–October) sea level anomalies relative to the long-term annual mean during 1993–2012 (the altimetry data). Note that hurricanes tend to intensify rapidly when passing over the high DSL/OHC regions in the Gulf of Mexico.

associated with the initial weakening of the AMOC (Fig. 4b and Fig. S8). Meanwhile, DSL rises in the Slope Sea, the Sargasso Sea, and the Gulf of Mexico, as well as along the U.S. Southeast and Gulf Coasts. The pattern of these contrast changes in DSL resembles the observed since 1993 (Fig. 4a), although the magnitude is generally larger in the model simulation.

In response to a further increase in the greenhouse gas forcing and a more significant reduction of the AMOC on centennial time scales (1993–2099) (Fig. S8), the DSL change pattern in the

model simulation and projection is somewhat different from that in 1993–2021 (Yin and Goddard 2013). The U.S. Northeast coast (and also the east coast of Canada) experiences the largest rise in DSL at a linear rate of 17 cm century^{-1} (Fig. 4c) (Hu et al. 2009; Yin et al. 2009; Little et al. 2019; Lyu et al. 2020; Yin et al. 2020). The DSL fall in the Eastern Subpolar Gyre is still present but less pronounced, and it extends southward into the Sargasso Sea south of the Gulf Stream. Thus, in response to the twenty-first-century greenhouse gas forcing, the pattern
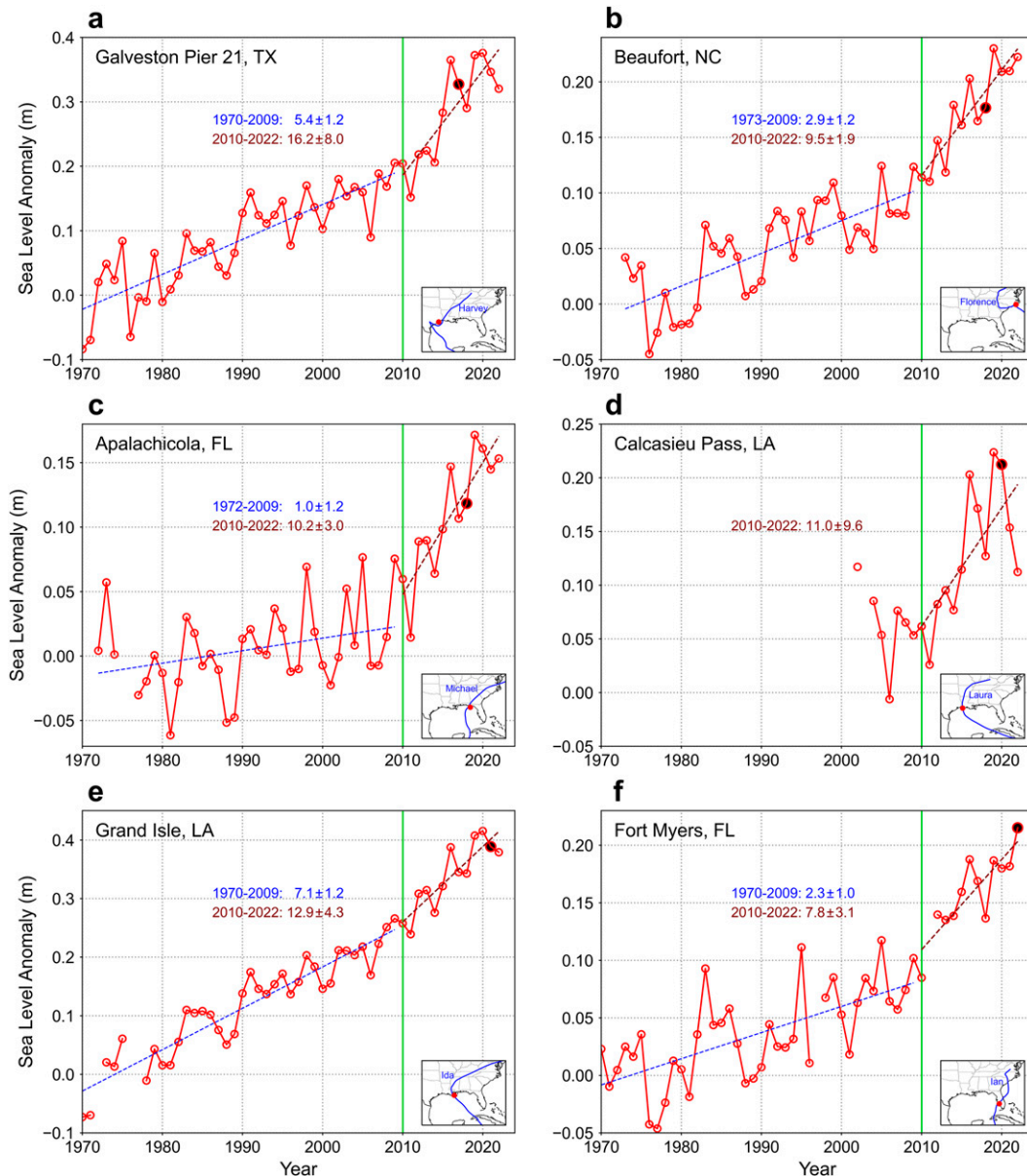
FIG. 12. 2010–22 acceleration of the relative SLR at six tide gauge stations along the Southeast and Gulf Coasts. (a) Galveston Pier 21, TX; (b) Beaufort, NC; (c) Apalachicola, FL; (d) Calcasieu Pass, LA; (e) Grand Isle, LA; and (f) Fort Myers, FL. The blue and brown dashed lines indicate the linear trends during 1970–2009 and 2010–22, respectively. The numbers are the mean rise rate (mm yr^{-1}) and its 95% confidence interval. The inset shows the location of the station (the red dot) and storm track of the six high-impact hurricanes since 2017 (the blue trajectory). The sea level for the year of the hurricane landfall is highlighted by the black dot with a larger size. Note that the long-term SLR data are not available at Calcasieu Pass in (d).

of DSL changes in the North Atlantic is not stationary but time evolving. The altimetry data of about 30 years thus far may not sufficiently reveal the pattern of centennial DSL changes.

d. Impact of the SLR acceleration on hurricane-induced storm surge along the Southeast and Gulf Coasts

The rapid SLR acceleration during 2010–22 has exacerbated recent hurricane-induced storm surge and coastal flooding especially along the Gulf Coast (Figs. 11–13). The acceleration coincided with active and even record-breaking North Atlantic hurricane seasons since 2016 (Fig. 11). In 2020, for example, a record of 30 named tropical cyclones formed in the North Atlantic (Fig. 11d) (Klotzbach et al. 2022). Among them, five hurricanes struck the Gulf Coast and caused significant, severe, to catastrophic coastal flooding and damages (NOAA 2022).
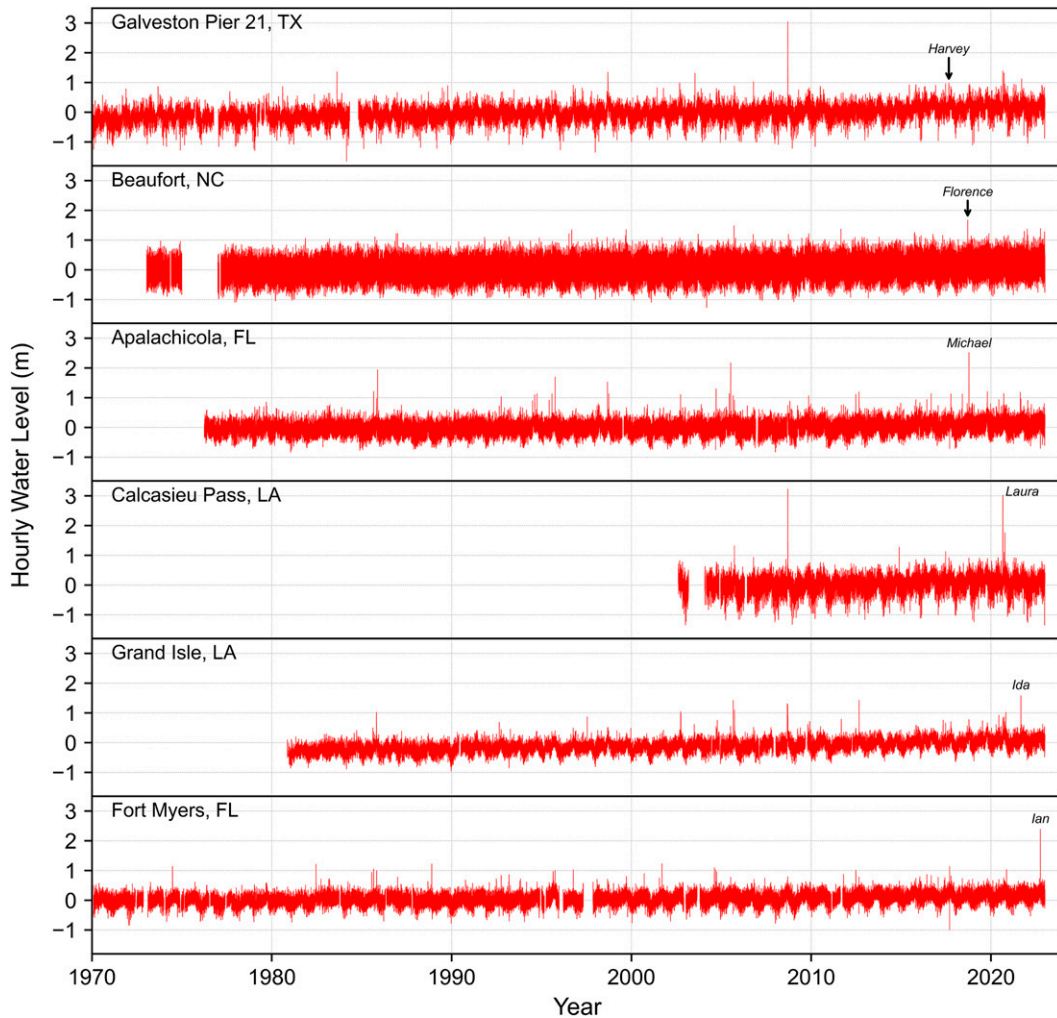
FIG. 13. Observed hourly water levels since 1970 at the six tide gauge stations along the Southeast and Gulf Coasts. The extreme water levels induced by the six high-impact hurricanes in the past six years are marked. The datum is chosen as the mean sea level during the 1983–2001 epoch for most stations. The long-term SLR is included.

On one hand, due to the rapid acceleration, the mean sea level on the Southeast and eastern Gulf Coasts has increased by about 0.1 m over the past decade (Figs. 2c,d and 5a). The 2010–22 SLR acceleration at individual tide gauge stations (Beaufort, Apalachicola, and Fort Myers) is similar to the regional mean (Figs. 12b,c,f). Relative SLR also accelerated on the western Gulf Coast such as at Galveston, Calcasieu Pass, and Grand Isle (Figs. 12a,d,e). The magnitude of the decadal SLR is comparable to the seasonal cycle amplitude of the coastal sea level (Fig. S9) and also to the tidal cycle amplitude on the Gulf Coast (Fig. 14).

Figure 15 shows that in the past six years, Hurricanes Harvey, Florence, Michael, Laura, Ida, and Ian caused 0.7, 1.6, 2.4, 2.5, 1.6, and 2.1 m storm surge at the tide gauge stations of Galveston, Beaufort, Apalachicola, Calcasieu Pass, Grand Isle, and Fort Myers, respectively. These extreme storm surges occurred on a higher background sea level compared with a decade ago (Fig. 15). So just like high tides during the warm

season, higher mean sea levels could amplify storm surge nonlinearly (see appendix B for more discussion on storm surge and its impact factors) (Pugh 1987; Rego and Li 2010; Tebaldi et al. 2012; Ezer and Atkinson 2014). Due to the combined effect of SLR and storm surge, the observed hourly water levels at Beaufort, Apalachicola, Grand Isle, and Fort Myers reached the highest in Fig. 13 during the landfall of Hurricanes Florence, Michael, Ida, and Ian, respectively. The water level associated with Hurricane Laura was the second highest at Calcasieu Pass. The impact of the slow-moving Hurricane Harvey was mainly on surge duration (4–5 days) rather than surge height at Galveston (Fig. 15a). The SLR component in extreme events will continue to grow in the future (Sweet et al. 2022).

On the other hand, the higher DSL in the Gulf of Mexico means higher ocean heat content (OHC) and hurricane heat potential (Leipper and Volgenau 1972). More energy and moisture could be supplied to the landfalling hurricanes (Risser and
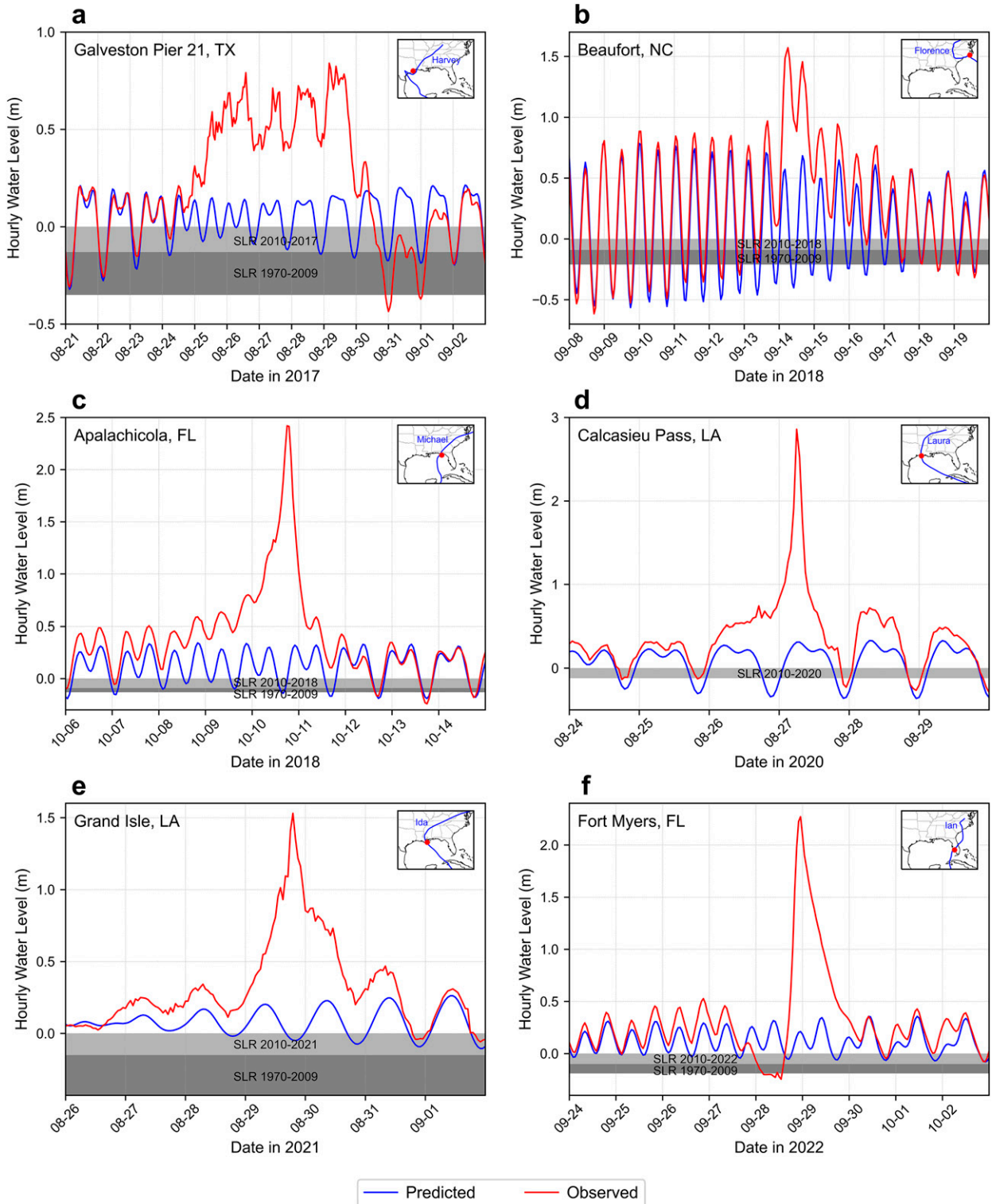
FIG. 14. Predicted and observed hourly waters levels at the six stations during the landfall of the six hurricanes. The long-term SLR is removed in the red and blue curves. The gray shadings show the SLR magnitudes during 1970–2009 and since 2010. They are calculated based on the linear trends of the tide gauge data (Fig. 12). (a) Galveston Pier 21 during Hurricane Harvey in 2017; (b) Beaufort during Hurricane Florence in 2018; (c) Apalachicola during Hurricane Michael in 2018; (d) Calcasieu Pass during Hurricane Laura in 2020; (e) Grand Isle during Hurricane Ida in 2021; and (f) Fort Myers during Hurricane Ian in 2022. The inset shows the location of the station (the red dot) and storm track of the hurricane (the blue trajectory).
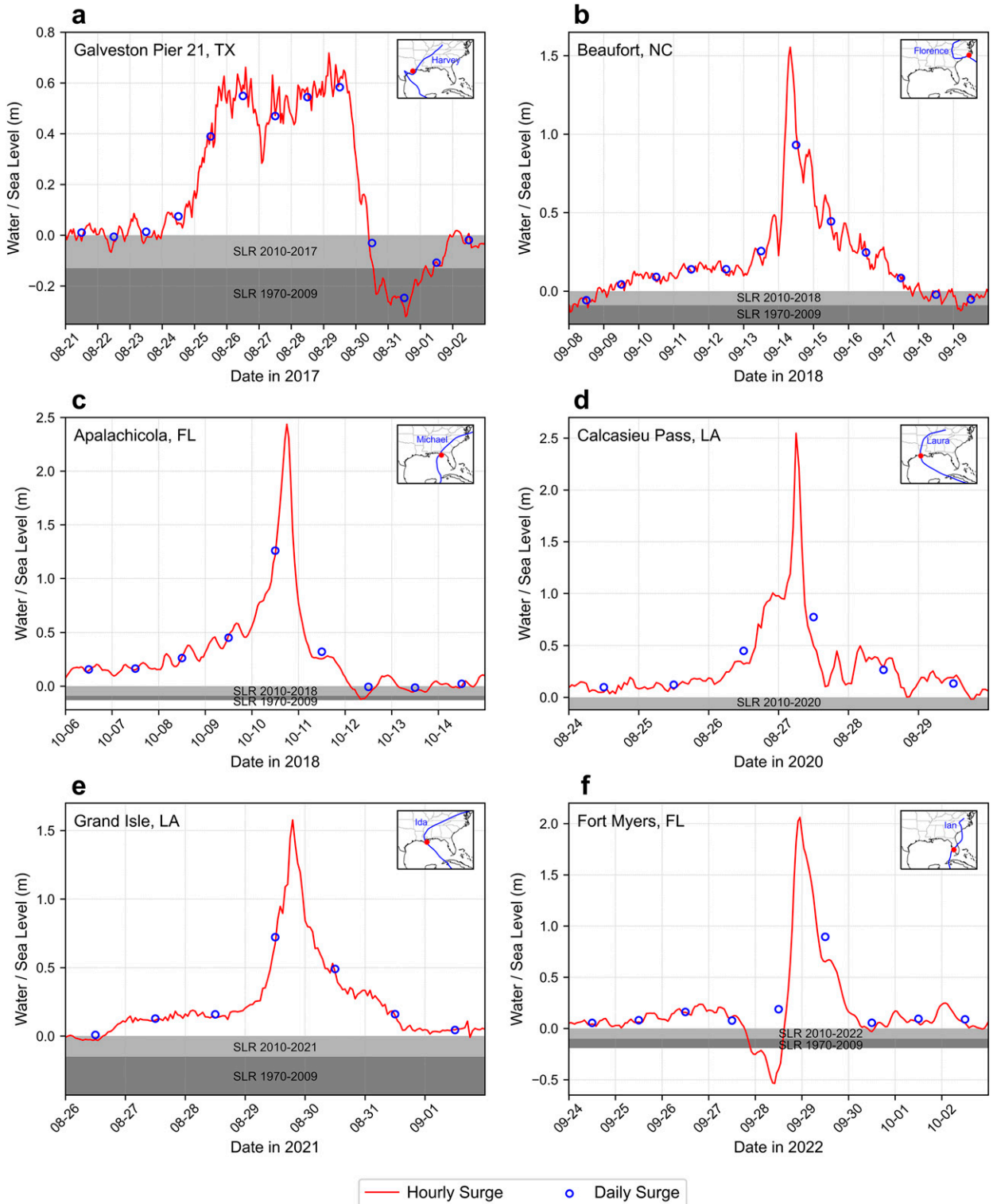
FIG. 15. The 2010–22 SLR acceleration leading to elevated storm surge during recent hurricanes. (a) Galveston Pier 21 during Hurricane Harvey in 2017; (b) Beaufort during Hurricane Florence in 2018; (c) Apalachicola during Hurricane Michael in 2018; (d) Calcasieu Pass during Hurricane Laura in 2020; (e) Grand Isle during Hurricane Ida in 2021; and (f) Fort Myers during Hurricane Ian in 2022. The red curve shows the hurricane-induced storm surge (i.e., the difference between the predicted and observed water levels in Fig. 14). Blue circles are the daily mean of the hourly storm surge data, measuring the combined effect of surge height and duration. The gray shadings show the SLR magnitudes during 1970–2009 and since 2010. They are calculated based on the linear trends of the tide gauge data (Fig. 12). The inset shows the location of the station (the red dot) and storm track of the hurricane (the blue trajectory). Note that the long-term SLR data are not available at Calcasieu Pass in (d).

Wehner 2017; Trenberth et al. 2018). Indeed, hurricanes tend to intensify rapidly when passing over anomalously high DSL/OHC regions in the Gulf, especially during the recent years associated with the high-impact Hurricanes Harvey, Michael, Laura, Ida, and Ian (Fig. 11) (Potter et al. 2019; Eley et al. 2021; Le Hénaff et al. 2021). The thicker layer of warm waters in the upper ocean and the associated high DSL limit the cold wake left behind by storms and therefore reduce its weakening effect on the hurricane intensity. Despite its potential role, an in-depth study on the AMOC–hurricane interaction is beyond the scope of the present study, but nonetheless an interesting topic for the follow-up research.

4. Discussion and conclusions

With the century-long tide gauge data and the more recent altimetry data, we focus on the rapid acceleration of SLR during 2010–22 on the U.S. Southeast and Gulf Coasts (Wdowinski et al. 2016; Valle-Levinson et al. 2017; Domingues et al. 2018; Ezer 2019). This acceleration is characterized by a >10 mm yr^{-1} decadal rise rate, multiple years with a ≥3σ sea level departure from the long-term trend, and the sea level records being broken more frequently (Figs. 2 and 3).

Compared with previous decadal SLR, the recent one was unprecedented in several ways. For example, the decadal SLR during 1936–48 on the Southeast coast was mainly driven by the extreme high sea level in 1948 (>3σ departure from the linear trend), followed by a drastic sea level drop in 1949–50 (Figs. 2c and 3c). So the 1936–48 SLR was likely caused by short, transient processes such as the wind (De Veaux 1955). By contrast, the SLR acceleration during 2010–22 is less sensitive to any individual year and represents the overall behavior of sea level during the decade. This is evident by the decadal running mean curves in Fig. 3, which show the sea level departure in the recent decade being the largest and highest.

Our mechanism analysis indicates that the atmospheric forcing was not the main cause of the 2010–22 acceleration. Instead, the acceleration is the coastal manifestation of the large-scale DSL adjustment to the observed 2009–10 AMOC slowdown. Since the occurrence of the slowdown event, more than a decade has passed. With more years' data becoming available, the impact of the event on the coastal sea level can be seen more clearly now. According to Fig. 8, the AMOC only partially recovered after 2010. Namely, the AMOC volume transport reduced by 2.1 Sv (1 Sv ≡ 10^6 m^3 s^{-1}) and from 18.6 Sv during 2004–08 down to 16.5 Sv during 2011–20. The adjustment of DSL to the AMOC variability and change can be through both barotropic and baroclinic processes (Lowe and Gregory 2006). While the former process is relatively fast, the latter process associated with ocean density change and heat redistribution can take longer time (Bryden et al. 2020).

The role of the AMOC in the SLR acceleration on the Southeast coast was ruled out in the previous study (Valle-Levinson et al. 2017). It was because previous climate models projected a rise in DSL on the Northeast rather than the Southeast coast, associated with the AMOC weakening over the twenty-first century (Yin et al. 2009). However, the latest climate model with refined resolutions and improved physics and dynamics indeed captures the observed pattern of contrast changes in DSL over the satellite era (1993–2021)—a fall in the Eastern Subpolar Gyre and a rise along the Southeast and Gulf Coasts (Fig. 4). This pattern is highly indicative of AMOC's important role in the SLR acceleration.

If the 2009–10 AMOC slowdown event turns out to be a part of a long-term weakening trend, as projected by climate models under greenhouse gas forcing (Fig. S8) (Weijer et al. 2020; Yin et al. 2020), sea levels along the East and Gulf Coasts may stay high in the next years (Figs. 2 and 3). Nonetheless, it is likely that the rapid SLR along the Southeast and Gulf Coasts, at a rate of more than 10 mm yr^{-1} during 2010–22, will taper off in the next decade. In other words, the 2009–10 AMOC slowdown carves notable, decadal features on the long-term sea level curves in Fig. 2. In a warming climate, these abnormal sea level behaviors in every new decade are valuable to early detect the increasing anthropogenic influence on sea level and ocean circulation from their background variability.

Data availability statement. All the observational and reanalysis data can be accessed from the websites listed in Table 1. The GFDL CM4 simulation and projection data can be accessed at the CMIP6 archive (https://esgf-node.llnl.gov/projects/cmip6/).

APPENDIX A

Dynamic Sea Level and Its Components

DSL is the departure of sea surface height from the geoid (Griffies et al. 2014; Gregory et al. 2019). By definition, it always has a zero global mean and reflects spatial patterns of sea level and sea level change. The DSL change can be caused by local changes in ocean density and mass. In the ocean interior, the steric effect dominates the DSL change (Fig. S6). For the Levitus data, the steric, thermosteric, and halosteric sea levels are computed based on three-dimensional ocean temperature and salinity data (Antonov et al. 2002):

$$SSL_{thermo}(x, y, t) = \int_{z1}^{z2} \frac{1}{\alpha}\frac{\partial \alpha}{\partial T} \Delta T dz, \tag{A1}$$

$$SSL_{halo}(x, y, t) = \int_{z1}^{z2} \frac{1}{\alpha}\frac{\partial \alpha}{\partial S} \Delta S \, dz, \quad \text{and} \tag{A2}$$

$$SSL(x, y, t) = SSL_{thermo}(x, y, t) + SSL_{halo}(x, y, t), \tag{A3}$$

where SSL is the steric sea level; SSL_{thermo} and SSL_{halo} are its thermosteric and halosteric components, respectively; T, S, z,

and α are ocean temperature, salinity, depth, and specific volume, respectively.

To compare DSL from the altimetry data with the steric sea level from the in situ data, the global mean of SSL needs to be removed:

$$\text{SSL}'(x, y, t) = \text{SSL}(x, y, t) - \overline{\text{SSL}}(t), \qquad \text{(A4)}$$

where the overbar and prime terms denote the global mean and local deviation, respectively. Same calculation and notation apply to $\text{SSL}'_{\text{thermo}}$ and $\text{SSL}'_{\text{halo}}$.

APPENDIX B

Extreme Coastal Water Level and Its Components

Coastal damages during hurricane-induced storm surge critically depend on how high the water can reach, how long the high water level can last, and how far it can intrude inland. The highest water level ($\hat{h}$), occurring over seconds, minutes, hours, or even days, is a result of the combined effect and complex interactions of various factors and processes operating on very different time scales (Ezer and Atkinson 2014; Sweet et al. 2022).

$$\hat{h} = \underbrace{\overline{\text{SL}}}_{} + \underbrace{\text{SLR}}_{\substack{0.1\,\text{m} \\ \text{over 2010--22}}} + \underbrace{\widetilde{\text{SL}}}_{\substack{0.1\,\text{m} \\ \text{amplitude}}} + \underbrace{\text{Tide}}_{\substack{0.1\text{--}0.3\,\text{m} \\ \text{amplitude}}} + \underbrace{\text{Surge}}_{\substack{0.7\text{--}2.5\,\text{m}}} + \text{Wave} + \text{Other}. \qquad \text{(B1)}$$

$$\underbrace{}_{\substack{\text{years} \\ \text{decades} \\ \text{centuries}}} \quad \underbrace{}_{\text{months}} \quad \underbrace{}_{\text{hours}} \quad \underbrace{}_{\substack{\text{minutes} \\ \text{hours} \\ \text{days}}} \quad \underbrace{}_{\text{seconds}}$$

The terms on the right-hand side of Eq. (B1) differ in nature, as they could represent different cycles, or gradual, persistent, and long-term trends, or short, transient, and strong fluctuations of coastal sea/water levels. Equation (B1) compares their relative magnitudes/amplitudes and highlights their distinct time scales of operation.

The $\overline{\text{SL}}$ term is the reference mean sea level at a particular location; SLR is the rise in the mean sea level. It can be further decomposed into global, regional, and local contributions. According to Fig. 2, the mean sea level along the Southeast and eastern Gulf Coasts has risen by more than 0.3 m over the past 100 years, and by more than 0.1 m during 2010–22. On the mid-Atlantic and western Gulf Coasts, land subsidence could contribute significantly to the faster SLR rates (Karegar et al. 2016; Buzzanga et al. 2020; Wang et al. 2020). Under climate change, the SLR term will continue to increase in the future (Sweet et al. 2022).

The $\widetilde{\text{SL}}$ term denotes the seasonal cycle of the coastal sea level. In a 1-yr period, sea level along the Southeast and Gulf Coasts is lowest in January and highest around September (Fig. S9). The amplitude of the seasonal cycle is about 0.1 m (i.e., the sea level departure in January or September relative to the annual mean). It is caused by seasonal heating and cooling of the ocean from the surface, and seasonal changes in ocean currents, atmospheric winds, and pressure. For example, high coastal sea levels during September–October are related to the seasonal decline of the Florida Current/Gulf Stream transport from its peak value in July (Stumpf and Haines 1998). In addition, the annual and semiannual tides have a large contribution to the seasonal sea level cycle along the East Coast (Ezer 2020). August–October are also the peak months of hurricane activities in the North Atlantic and the Gulf of Mexico.

Storm surge, defined as the difference between the predicted and observed water levels during the hurricane landfall, is one largest term in Eq. (B1). The "Surge" term consists of a wind surge and a pressure surge component, with the former dominant. The height and duration of the peak surge critically depend on storm characteristics including intensity, frequency, size, path, translation speed, and landfall angle. Among the six major hurricanes surveyed here, the peak hourly surge ranges from 0.7 to 2.5 m (Fig. 15).

Tides are mixed semidiurnal on the eastern Gulf Coast and diurnal on the western Gulf Coast (Fig. 14). The tidal range around the Gulf of Mexico is generally smaller than other coastal regions. The amplitude varies from 0.1 to 0.3 m (i.e., the high/low tide relative to the mean sea level). Ocean waves are filtered out in the tide gauge data. But they could be an important factor in causing coastal flooding and damage. The "Other" term in Eq. (B1) denotes all other processes or effects such as the nonlinear (constructive or destructive) interactions among the tide, surge, wave, rising mean sea level, etc. (Pugh 1987; Rego and Li 2010; Wu et al. 2018)

REFERENCES

Antonov, J. I., S. Levitus, and T. P. Boyer, 2002: Steric sea level variations during 1957–1994: Importance of salinity. *J. Geophys. Res.*, **107**, 8013, https://doi.org/10.1029/2001JC000964.

Bryden, H. L., B. A. King, G. D. McCarthy, and E. L. McDonagh, 2014: Impact of a 30% reduction in Atlantic meridional overturning during 2009–2010. *Ocean Sci.*, **10**, 683–691, https://doi.org/10.5194/os-10-683-2014.

——, W. E. Johns, B. A. King, G. McCarthy, E. L. McDonagh, B. I. Moat, and D. A. Smeed, 2020: Reduction in ocean heat transport at 26°N since 2008 cools the Eastern Subpolar Gyre of the North Atlantic Ocean. *J. Climate*, **33**, 1677–1689, https://doi.org/10.1175/JCLI-D-19-0323.1.

Buzzanga, B., D. P. Bekaert, B. D. Hamlington, and S. S. Sangha, 2020: Toward sustained monitoring of subsidence at the coast using InSAR and GPS: An application in Hampton Roads,

Virginia. *Geophys. Res. Lett.*, **47**, e2020GL090013, https://doi.org/10.1029/2020GL090013.

Chafik, L., J. E. Ø. Nilsen, S. Dangendorf, G. Reverdin, and T. Frederikse, 2019: North Atlantic Ocean circulation and decadal sea level change during the altimetry era. *Sci. Rep.*, **9**, 1041, https://doi.org/10.1038/s41598-018-37603-6.

Chemke, R., L. Zanna, and L. M. Polvani, 2020: Identifying a human signal in the North Atlantic warming hole. *Nat. Commun.*, **11**, 1540, https://doi.org/10.1038/s41467-020-15285-x.

De Veaux, E. J., 1955: Meteorological trend and the apparent rise in sea level along the South Carolina Coast. *Mon. Wea. Rev.*, **83**, 217–224, https://doi.org/10.1175/1520-0493(1955)083<0217:MTATAR>2.0.CO;2.

Domingues, R., G. Goni, M. Baringer, and D. Volkov, 2018: What caused the accelerated sea level changes along the U.S. East Coast during 2010–2015? *Geophys. Res. Lett.*, **45**, 13 367–13 376, https://doi.org/10.1029/2018GL081183.

Douglas, B. C., M. S. Kearney, and S. P. Leatherman, 2001: *Sea Level Rise History and Consequences*. Academic Press, 232 pp.

Eley, E. N., B. Subrahmanyam, and C. B. Trott, 2021: Ocean–atmosphere interactions during Hurricanes Marco and Laura (2020). *Remote Sens.*, **13**, 1932, https://doi.org/10.3390/rs13101932.

Eyring, V., S. Bony, G. A. Meehl, C. A. Senior, B. Stevens, R. J. Stouffer, and K. E. Taylor, 2016: Overview of the Coupled Model Intercomparison Project Phase 6 (CMIP6) experimental design and organization. *Geosci. Model Dev.*, **9**, 1937–1958, https://doi.org/10.5194/gmd-9-1937-2016.

Ezer, T., 2015: Detecting changes in the transport of the Gulf Stream and the Atlantic overturning circulation from coastal sea level data: The extreme decline in 2009–2010 and estimated variations for 1935–2012. *Global Planet. Change*, **129**, 23–36, https://doi.org/10.1016/j.gloplacha.2015.03.002.

——, 2019: Regional differences in sea level rise between the Mid-Atlantic Bight and the South Atlantic Bight: Is the Gulf Stream to blame? *Earth's Future*, **7**, 771–783, https://doi.org/10.1029/2019EF001174.

——, 2020: Analysis of the changing patterns of seasonal flooding along the U.S. East Coast. *Ocean Dyn.*, **70**, 241–255, https://doi.org/10.1007/s10236-019-01326-7.

——, and L. P. Atkinson, 2014: Accelerated flooding along the U.S. East Coast: On the impact of sea level rise, tides, storms, the Gulf Stream, and the North Atlantic Oscillations. *Earth's Future*, **2**, 362–382, https://doi.org/10.1002/2014EF000252.

Fasullo, J. T., and R. S. Nerem, 2018: Altimeter-era emergence of the patterns of forced sea-level rise in climate models and implications for the future. *Proc. Natl. Acad. Sci. USA*, **115**, 12 944–12 949, https://doi.org/10.1073/pnas.1813233115.

——, P. R. Gent, and R. S. Nerem, 2020: Sea level rise in the CESM large ensemble: The role of individual climate forcings and consequences for the coming decades. *J. Climate*, **33**, 6911–6927, https://doi.org/10.1175/JCLI-D-19-1001.1.

Goddard, P. B., J. J. Yin, S. M. Griffies, and S. Q. Zhang, 2015: An extreme event of sea-level rise along the northeast coast of North America in 2009–2010. *Nat. Commun.*, **6**, 6346, https://doi.org/10.1038/ncomms7346.

Gregory, J. M., and Coauthors, 2019: Concepts and terminology for sea level: Mean, variability and change, both local and global. *Surv. Geophys.*, **40**, 1251–1289, https://doi.org/10.1007/s10712-019-09525-z.

Griffies, S. M., and Coauthors, 2014: An assessment of global and regional sea level for years 1993–2007 in a suite of interannual CORE-II simulations. *Ocean Modell.*, **78**, 35–89, https://doi.org/10.1016/j.ocemod.2014.03.004.

Hamlington, B. D., and Coauthors, 2020: Understanding of contemporary regional sea-level change and the implications for the future. *Rev. Geophys.*, **58**, e2019RG000672, https://doi.org/10.1029/2019RG000672.

Harvey, T. C., and Coauthors, 2021: Ocean mass, sterodynamic effects, and vertical land motion largely explain US coast relative sea level rise. *Commun. Earth Environ.*, **2**, 233, https://doi.org/10.1038/s43247-021-00300-w.

Held, I. M., and Coauthors, 2019: Structure and performance of GFDL's CM4.0 climate model. *J. Adv. Model. Earth Syst.*, **11**, 3691–3727, https://doi.org/10.1029/2019MS001829.

Hersbach, H., and Coauthors, 2020: The ERA5 global reanalysis. *Quart. J. Roy. Meteor. Soc.*, **146**, 1999–2049, https://doi.org/10.1002/qj.3803.

Hu, A. X., G. A. Meehl, W. Q. Han, and J. J. Yin, 2009: Transient response of the MOC and climate to potential melting of the Greenland Ice Sheet in the 21st century. *Geophys. Res. Lett.*, **36**, L10707, https://doi.org/10.1029/2009GL037998.

IPCC, 2021: *Climate Change 2021: The Physical Science Basis*. Cambridge University Press, 2391 pp., https://www.ipcc.ch/report/ar6/wg1/downloads/report/IPCC_AR6_WGI_FullReport.pdf.

Johns, W. E., and Coauthors, 2011: Continuous, array-based estimates of Atlantic Ocean heat transport at 26.5°N. *J. Climate*, **24**, 2429–2449, https://doi.org/10.1175/2010JCLI3997.1.

Karegar, M. A., T. H. Dixon, and S. E. Engelhart, 2016: Subsidence along the Atlantic Coast of North America: Insights from GPS and late Holocene relative sea level data. *Geophys. Res. Lett.*, **43**, 3126–3133, https://doi.org/10.1002/2016GL068015.

Klotzbach, P. J., and Coauthors, 2022: A hyperactive end to the Atlantic hurricane season October–November 2020. *Bull. Amer. Meteor. Soc.*, **103**, E110–E128, https://doi.org/10.1175/BAMS-D-20-0312.1.

Knapp, K. R., M. C. Kruk, D. H. Levinson, H. J. Diamond, and C. J. Neumann, 2010: The International Best Track Archive for Climate Stewardship (IBTrACS) unifying tropical cyclone data. *Bull. Amer. Meteor. Soc.*, **91**, 363–376, https://doi.org/10.1175/2009BAMS2755.1.

——, H. J. Diamond, J. P. Kossin, M. C. Kruk, and C. J. Schreck, 2018: International Best Track Archive for Climate Stewardship (IBTrACS) project, version 4. NOAA National Centers for Environmental Information, accessed 30 December 2022, https://doi.org/10.25921/82ty-9e16.

Le Hénaff, M., and Coauthors, 2021: The role of the Gulf of Mexico ocean conditions in the intensification of Hurricane Michael (2018). *J. Geophys. Res. Oceans*, **126**, e2020JC016969, https://doi.org/10.1029/2020JC016969.

Leipper, D. F., and D. Volgenau, 1972: Hurricane heat potential of the Gulf of Mexico. *J. Phys. Oceanogr.*, **2**, 218–224, https://doi.org/10.1175/1520-0485(1972)002<0218:HHPOTG>2.0.CO;2.

Levitus, S., and Coauthors, 2012: World ocean heat content and thermosteric sea level change (0–2000 m), 1955–2010. *Geophys. Res. Lett.*, **39**, L10603, https://doi.org/10.1029/2012GL051106.

Little, C. M., A. Hu, C. W. Hughes, G. D. McCarthy, C. G. Piecuch, R. M. Ponte, and M. D. Thomas, 2019: The relationship between U.S. East Coast sea level and the Atlantic meridional overturning circulation: A review. *J. Geophys. Res. Oceans*, **124**, 6435–6458, https://doi.org/10.1029/2019JC015152.

——, C. G. Piecuch, and R. M. Ponte, 2021: North American east coast sea level exhibits high power and spatiotemporal complexity on decadal timescales. *Geophys. Res. Lett.*, **48**, e2021GL093675, https://doi.org/10.1029/2021GL093675.

Lowe, J. A., and J. M. Gregory, 2006: Understanding projections of sea level rise in a Hadley Centre coupled climate model. *J. Geophys. Res.*, **111**, C11014, https://doi.org/10.1029/2005JC003421.

Lyu, K., X. Zhang, and J. A. Church, 2020: Regional dynamic sea level simulated in the CMIP5 and CMIP6 models: Mean biases, future projections, and their linkages. *J. Climate*, **33**, 6377–6398, https://doi.org/10.1175/JCLI-D-19-1029.1.

McCarthy, G. D., and Coauthors, 2015: Measuring the Atlantic meridional overturning circulation at 26°N. *Prog. Oceanogr.*, **130**, 91–111, https://doi.org/10.1016/j.pocean.2014.10.006.

Neto, A. G., J. A. Langan, and J. B. Palter, 2021: Changes in the Gulf Stream preceded rapid warming of the northwest Atlantic shelf. *Commun. Earth Environ.*, **2**, 74, https://doi.org/10.1038/s43247-021-00143-5.

NOAA, 2022: U.S. billion-dollar weather and climate disasters. NCDC, https://www.ncdc.noaa.gov/billions/.

O'Neill, B. C., and Coauthors, 2016: The Scenario Model Intercomparison Project (ScenarioMIP) for CMIP6. *Geosci. Model Dev.*, **9**, 3461–3482, https://doi.org/10.5194/gmd-9-3461-2016.

Pershing, A. J., and Coauthors, 2015: Slow adaptation in the face of rapid warming leads to collapse of the Gulf of Maine cod fishery. *Science*, **350**, 809–812, https://doi.org/10.1126/science.aac9819.

Piecuch, C. G., and R. M. Ponte, 2015: Inverted barometer contributions to recent sea level changes along the northeast coast of North America. *Geophys. Res. Lett.*, **42**, 5918–5925, https://doi.org/10.1002/2015GL064580.

Potter, H., S. F. DiMarco, and A. H. Knap, 2019: Tropical cyclone heat potential and the rapid intensification of Hurricane Harvey in the Texas Bight. *J. Geophys. Res. Oceans*, **124**, 2440–2451, https://doi.org/10.1029/2018JC014776.

Pugh, D. T., 1987: *Tides, Surges and Mean Sea Level*. John Wiley and Sons, 472 pp.

Pujol, M.-I., Y. Faugère, G. Taburet, S. Dupuy, C. Pelloquin, M. Ablain, and N. Picot, 2016: DUACS DT2014: The new multimission altimeter data set reprocessed over 20 years. *Ocean Sci.*, **12**, 1067–1090, https://doi.org/10.5194/os-12-1067-2016.

Rahmstorf, S., J. E. Box, G. Feulner, M. E. Mann, A. Robinson, S. Rutherford, and E. J. Schaffernicht, 2015: Exceptional twentieth-century slowdown in Atlantic Ocean overturning circulation. *Nat. Climate Change*, **5**, 475–480, https://doi.org/10.1038/nclimate2554.

Rego, J. L., and C. Li, 2010: Nonlinear terms in storm surge predictions: Effect of tide and shelf geometry with case study from Hurricane Rita. *J. Geophys. Res.*, **115**, C06020, https://doi.org/10.1029/2009JC005285.

Reidmiller, D. R., C. W. Avery, D. R. Easterling, K. E. Kunkel, K. L. M. Lewis, T. K. Maycock, and B. C. Stewart, Eds., 2018: *Impacts, Risks, and Adaptation in the United States*. Vol. II, *Fourth National Climate Assessment*, U.S. Global Change Research Program, 1515 pp., https://doi.org/10.7930/NCA4.2018.

Risser, M. D., and M. F. Wehner, 2017: Attributable human-induced changes in the likelihood and magnitude of the observed extreme precipitation during Hurricane Harvey. *Geophys. Res. Lett.*, **44**, 12 457–12 464, https://doi.org/10.1002/2017GL075888.

Sallenger, A. H., K. S. Doran, and P. A. Howd, 2012: Hotspot of accelerated sea-level rise on the Atlantic coast of North America. *Nat. Climate Change*, **2**, 884–888, https://doi.org/10.1038/nclimate1597.

Simpson, R. H., and H. Saffir, 1974: The hurricane disaster-potential scale. *Weatherwise*, **27**, 169–186, https://doi.org/10.1080/00431672.1974.9931702.

Smeed, D. A., and Coauthors, 2014: Observed decline of the Atlantic meridional overturning circulation 2004–2012. *Ocean Sci.*, **10**, 29–38, https://doi.org/10.5194/os-10-29-2014.

Stumpf, R., and J. Haines, 1998: Variations in tidal level in the Gulf of Mexico and implications for tidal wetlands. *Estuarine Coastal Shelf Sci.*, **46**, 165–173, https://doi.org/10.1006/ecss.1997.0276.

Sweet, W. V., S. Simon, G. Dusek, D. Marcy, W. Brooks, M. Pendleton, and J. Marra, 2021: 2021 state of high tide flooding and annual outlook. NOAA High Tide Flooding Rep., 28 pp., https://tidesandcurrents.noaa.gov/publications/2021_State_of_High_Tide_Flooding_and_Annual_Outlook_Final.pdf.

——, and Coauthors, 2022: Global and regional sea level rise scenarios for the United States: Updated mean projections and extreme water level probabilities along U.S. coastlines. NOAA Tech. Rep. NOS 01, 111 pp., https://www.astro.sunysb.edu/fwalter/HON301/noaa-nos-techrpt01-global-regional-SLR-scenarios-US.pdf.

Taburet, G., A. Sanchez-Roman, M. Ballarotta, M.-I. Pujol, J.-F. Legeais, F. Fournier, Y. Faugere, and G. Dibarboure, 2019: DUACS DT2018: 25 years of reprocessed sea level altimetry products. *Ocean Sci.*, **15**, 1207–1224, https://doi.org/10.5194/os-15-1207-2019.

Tebaldi, C., B. H. Strauss, and C. E. Zervas, 2012: Modelling sea level rise impacts on storm surges along US coasts. *Environ. Res. Lett.*, **7**, 014032, https://doi.org/10.1088/1748-9326/7/1/014032.

Trenberth, K. E., L. Cheng, P. Jacobs, Y. Zhang, and J. Fasullo, 2018: Hurricane Harvey links to ocean heat content and climate change adaptation. *Earth's Future*, **6**, 730–744, https://doi.org/10.1029/2018EF000825.

Valle-Levinson, A., A. Dutton, and J. B. Martin, 2017: Spatial and temporal variability of sea level rise hot spots over the eastern United States. *Geophys. Res. Lett.*, **44**, 7876–7882, https://doi.org/10.1002/2017GL073926.

Wang, G., X. Zhou, K. Wang, X. Ke, Y. Zhang, R. Zhao, and Y. Bao, 2020: GOM20: A stable geodetic reference frame for subsidence, faulting, and sea-level rise studies along the coast of the Gulf of Mexico. *Remote Sens.*, **12**, 350, https://doi.org/10.3390/rs12030350.

Wang, J., J. A. Church, X. Zhang, and X. Chen, 2021: Reconciling global mean and regional sea level change in projections and observations. *Nat. Commun.*, **12**, 990, https://doi.org/10.1038/s41467-021-21265-6.

Wdowinski, S., R. Bray, B. P. Kirtman, and Z. Wu, 2016: Increasing flooding hazard in coastal communities due to rising sea level: Case study of Miami Beach, Florida. *Ocean Coastal Manage.*, **126**, 1–8, https://doi.org/10.1016/j.ocecoaman.2016.03.002.

Weijer, W., W. Cheng, O. A. Garuba, A. Hu, and B. Nadiga, 2020: CMIP6 models predict significant 21st century decline of the Atlantic meridional overturning circulation. *Geophys. Res. Lett.*, **47**, e2019GL086075, https://doi.org/10.1029/2019GL086075.

Wu, G., F. Shi, J. T. Kirby, B. Liang, and J. Shi, 2018: Modeling wave effects on storm surge and coastal inundation. *Coastal Eng.*, **140**, 371–382, https://doi.org/10.1016/j.coastaleng.2018.08.011.

Wuebbles, D. J., D. W. Fahey, K. A. Hibbard, D. J. Dokken, B. C. Stewart, and T. K. Maycock, Eds., 2017: *Climate Science Special Report*. Vol. I, *Fourth National Climate Assessment*, U.S. Global Change Research Program, 470 pp., https://doi.org/10.7930/J0J964J6.

Yin, J., and P. B. Goddard, 2013: Oceanic control of sea level rise patterns along the East Coast of the United States. *Geophys. Res. Lett.*, **40**, 5514–5520, https://doi.org/10.1002/2013GL057992.

——, M. E. Schlesinger, and R. J. Stouffer, 2009: Model projections of rapid sea-level rise on the northeast coast of the United States. *Nat. Geosci.*, **2**, 262–266, https://doi.org/10.1038/ngeo462.

——, S. M. Griffies, M. Winton, M. Zhao, and L. Zanna, 2020: Response of storm-related extreme sea level along the US Atlantic coast to combined weather and climate forcing. *J. Climate*, **33**, 3745–3769, https://doi.org/10.1175/JCLI-D-19-0551.1.

Zervas, C. E., 2001: Sea level variations of the United States 1854–1999. NOAA Tech. Rep. NOS CO-OPS 36, 201 pp., https://tidesandcurrents.noaa.gov/publications/NOAA_Technical_Report_NOS_COOPS_036.pdf.

——, 2009: Sea level variations of the United States, 1854–2006. NOAA Tech. Rep. NOS CO-OPS 053, 194 pp., https://tidesandcurrents.noaa.gov/publications/Tech_rpt_53.pdf.